PFC/RR-82-6

DOE/ET/51013-32
UC20 G

RADIAL EFFECTS IN HEATING AND THERMAL STABILITY OF A SUB-IGNITED TOKAMAK*

V. Fuchs[+], M. M. Shoucri[+], G. Thibaudeau[+]
L. Harten and A. Bers

February 1982

* Work supported in part by NSF Grant No. ENG 79-070947 and in part by DOE Contract No. DE-AC02-78ET-51013.

[+] Projet Tokamak de Varennes, Institut de Recherche d'Hydro-Quebec, Varennes, Quebec, Canada J0L 2P0.

ABSTRACT

The existence of thermally stable sub-ignited equilibria of a tokamak reactor, sustained in operation by a feedback-controlled supplementary heating source, is demonstrated. The establishment of stability depends on a number of radially non-uniform, nonlinear processes whose effect is analyzed. One-dimensional (radial) stability analyses of model transport equations, together with numerical results from a 1-D transport code, are used in studying the heating of DT-plasmas in the thermonuclear regime. Plasma core supplementary heating is found to be a thermally more stable process than bulk heating. In the presence of impurity line radiation, however, core-heated temperature profiles may collapse, contracting inward from the limiter, the result of an instability caused by the increasing nature of the radiative cooling rate, with decreasing temperature. Conditions are established for the realization of a sub-ignited high-Q, toroidal reactor plasma with appreciable output power (≈2 000 MW thermal).

1 INTRODUCTION

The subject of burn control of fusion plasmas is one of the major problems associated with reactor design and planning. The necessity for some form of control stems from the natural tendency of an ignited D-T plasma to self-accelerate the α-particle production rate beyond the point where the D-T reaction cross-section turns over. Heat production actually ceases when the α-particle deposition rate to the electrons and protons is outweighed by radiation and heat diffusion losses from the plasma. This typically occurs, if the reactor is not controlled, between 30 and 50 keV, a range of temperatures for which the neutron flux to the walls attains intolerable levels, and for which detrimental high-β induced MHD activity is likely to occur. Thus, the concensus so far[1] as regards the ideal operational range of tokamak plasma temperatures, T,and densities,n, is somewhere between $T = 10$ to 20 keV, and $n = 1$ to 5×10^{20} m^{-3}, subject to β and wall-loading constraints, typically $\beta \lesssim 10\%$ and a neutron flux of less then 2 MW/m^2.

A number of burn control methods have been proposed and discussed over the past few years, which, following Bromberg et al[2], can be appropriately divided into two distinct classes termed as active or passive burn control, depending, respectively, on whether or not information is fed back from the plasma to control some external agent which, in turn, directly controls the plasma state itself. As an example of active burn control we point out the currently popular idea of induced toroidal-field ripple resulting in enhanced α-particle deconfinement[3]. Evidently, the method achieves controlled reduction in the heating rate by effectively turning down the principal power

source, the α-particle heat deposition rate itself. Another natural candidate for control is the equally important supplementary power source[4,5] be it radio-frequency or neutral beam.

Quite obviously, as far as the problem of control is concerned, feedback onto an external heat source is the superior method, since it not only involves a shorter time delay in the feedback loop, but mainly one does not have to rely on whether an internal heat source is going to respond in a particular predicted manner.

The present work is essentially a stability study of steady high-Q (Q = power out/power in) tokamak reactor operation achieved by autonomous (i.e. via temperature) control of the supplementary heating source. The principal ideas, together with a proof of stability within a 0-D plasma transport representation, of this method of control were presented in Ref. 5. Here we go futher, examining the implications of radial effects on the stability with respect to small perturbations of the sub-ignited radial equilibria. The principal tools of our analysis are a criterion for the linear stability of equilibria of non-linear non-uniform parabolic partial differential equations due to Gelfand[6], and first used for plasma applications by Kolesnichenko[7] and Rosenau[8], and a 1-D (radial) transport code incorporating neo-classical ion heat transport but anomalous particle and electron heat transport consistent with ALCATOR-type scaling for the energy confinement time ($\tau_E \sim$ density).

Our main results are, first, the demonstration, according to the Gelfand

method, of asymptotic stability (i.e. stability with respect to small perturbations) of the equilibria created below ignition (i.e. where α-particle heating compensates all the losses) by a temperature-controlled turn-down of the supplementary heating source. Second, the successfull demonstration of stable sub-ignited operation using the 1-D (radial) transport code. Third, we present examples of radiative collapse of temperature profiles, specifically their contraction or inversion, in fact the manifestation of an instability caused by the generally decreasing character of impurity line radiation, as a function of temperature. Finally, we discuss the conditions for the realization of a commercially viable (≃ 2 000 MW thermal) high-Q tokamak reactor.

It is not the purpose of this study to carry out a systematic parameter study of tokamak thermal stability. Rather we select one particular configuration, which we refer to generically as RFDTR (Radio-Frequency Driven Tokamak Reactor) having parameters within the range of recent reactor designs[1,9]. The material is organized as follows. In section II we present the 1-D computational model for heat transfer. In section III, we discuss the problem of stability. One-dimensional time-evolution studies of the system are described in section IV. A reactor realization is discussed in section V, and finally, our conclusions make up section VI. All units throughout this work are MKS except for temperature T (keV), density $n[10^{20}\ m^{-3}]$ and thermal diffusivity $\kappa[10^{20}\ m^{-1}\ s^{-1}]$.

2 COMPUTATIONAL MODEL

We will examine our concept of creating stable sub-ignited tokamak equilibria through autonomous control of the supplementary heating source within the scope of a configuration that we refer to as RFDTR (Table 1).

The ALCATOR-A configuration is presented along with RFDTR not only for the sake of comparison, but because it will be employed as a benchmark case for testing our 1-D transport code, particularly as concerns the energy confinement time for which extensive experimental data are available[10]. The rationale for the choice of RFDTR parameters lies in the necessity to satisfy certain basic design criteria. Specifically, $q \gtrsim 1$ (see Eq. 16); $\beta \lesssim 10\%$ (in our units, average $\beta = 9.6 \times 10^4 \mu_o \langle nT \rangle / B^2 \simeq 5\%$), neutron flux to the wall ≤ 2 MW/m^2 (14 MeV neutrons produced at the average rate of the D-T reaction at $T_o = 15$ keV and at $n_o = 3 \times 10^{20}$ m^{-3}/wall area $\simeq 2$ MW/m^2), and at 6 MA an aspect ratio $R/a \gtrsim 4$ for at least 70% α-particle confinement[11,12]. The figure of 100 MW for the supplementary power is estimated in advance as that required to compensate for heat loss with an ALCATOR-scaling confinement time. We prefer RF heating over other possibilities, because of the ease and speed with which RF power sources can be controlled. Finally, if the configuration is to be a viable power-producing device, we must aim for at least 2 000 MW thermal at a Q (power out/power in) of about 50; this can be achieved with the large system (a = 2m, etc.). Results for a = 1.4m, etc., will illustrate the limitations on power out and Q which are associated with smaller systems.

In order to describe the evolution in time, t, and in the radial direction, r, of the ion and electron temperatures T_i and T_e, we solve the standard set of transport equations[13] somewhat simplified to serve our specific needs, using a predictor-corrector time-centered Crank-Nicolson scheme[14,15]. We require of the system that it obey the ALCATOR-type scaling law for the energy confinement time, $\tau_E \sim na^2$, but we allow for a reduction in τ_E as recently evidenced for devices where supplementary, rather than ohmic heating prevails[16]. This is achieved by numerically adjusting the anomalous electron heat conductivity. The major simplification of our code with respect to other larger tokamak transport codes is the absence of self-consistent particle recycling. Since a major part of our study consists in the examination of the system thermal stability in the peak density versus peak temperature space, we assume an equilibrium plasma density, characterized by a parabolic profile and an adjustable peak density.

The equations we consider are

$$2.4 \times 10^4 \frac{\partial nT_e}{\partial t} = 1.6 \times 10^4 \frac{1}{r} (r Q_e)' + P_{ohm} + f_e P_\alpha + g_e P_h - P_{rad} - P_{eq} \qquad (1a)$$

$$2.4 \times 10^4 \frac{\partial nT_i}{\partial t} = 1.6 \times 10^4 \frac{1}{r} (r Q_i)' + f_i P_\alpha + g_i P_h + P_{eq} \qquad (1b)$$

where $(...)' \equiv \partial/\partial r$, and the heat flux Q is taken as

$$Q_{e,i} = \kappa_{e,i} T'_{e,i} + \frac{3}{2} D T_{e,i} n' \qquad (2)$$

The relevant transport cofficients are ion neoclassical heat conductivity κ_i, electron anomalous heat conductivity κ_e, and particle anomalous diffusivity D. The ion neoclassical conductivity is

$$\kappa_i = n \rho_e^2 \nu_{ei} \left(\frac{m_i T_e}{m_e T_i}\right)^{\frac{1}{2}} \left[1 + 1.6\, q^2 + q^2 \left(\frac{R}{r}\right)^{3/2} \frac{0.68}{1 + 0.36\, \nu_i^*}\right] \quad (3)$$

a function which sharply decreases away from the plasma center. At r = 0,

$$\kappa_i\ (r \to o) = 8.55 \frac{n_o T_{io}^{3/2} q(o)}{B^2 R} \quad [10^{20}\ m^{-1}\ s^{-1}], \quad (4)$$

giving an appreciation of the neoclassical effect in the plasma core.

The neoclassical electron heat conductivity and particle diffusivity are scaled down with respect to κ_i by a factor of $(m_e/m_i)^{\frac{1}{2}}$. However, anomalous effects dominate electron heat and particle transport. In the absence, to date, of a definite theory of anomalous transport, there is some freedom to speculate about plausible expressions for the electron thermal conductivity. We limit ourselves to two simple models, compatible both numerically and as far as the scaling with density is concerned, with the ALCATOR-scaling confinement time[10] τ_E,

$$\tau_E = 0.32 \langle n \rangle a^2 q^{\frac{1}{2}}. \quad (5)$$

The first choice for κ_e is simply a constant, $\kappa_e \simeq 1$, the second is radially dependent via a $T^{\frac{1}{2}}$ term,

$$\kappa_e \simeq 1.5\ T_i^{\frac{1}{2}} \quad [10^{20}\ m^{-1}\ sec^{-1}], \quad (6)$$

consistent with recent theories[17, 18] of anomalous heat transport. To obtain the value of the particle diffusion coefficient D, we take into consideration the standard experimental observation that the particle confinement time exceeds the energy confinement time by roughly a factor of five. We hence take

$$D = 0.2\ \kappa_e/n \qquad [m^2/s], \tag{7}$$

to be applied in the expression (2) for the heat flux Q.

In Eq. (3), ρ_e is the electron Larmor radius

$$\rho_e = 7.525 \times 10^{-5}\ T_e^{\frac{1}{2}}/B \ , \tag{8}$$

with B the toroidal field. The collision frequency ν_{ei} is[19]

$$\nu_{ei} = 9.18 \times 10^3\ n\ Z_{eff}\ \ell n\ \Lambda/T_e^{3/2} \tag{9}$$

with $\Lambda = 1.1 \times 10^7\ T_e/n^{\frac{1}{2}}$, and ν_i^* is the ion collisionality parameter

$$\nu_i^* = 7.54 \times 10^{-8}\ \nu_{ei}\ Z_{eff}\ q\ \frac{R^{5/2}}{r^{3/2}}\ T_i^{-\frac{1}{2}} \ . \tag{10}$$

Further, q is the "safety factor"

$$q = \frac{r}{R}\ \frac{B}{B_p} \tag{11}$$

with B_p the poloidal field, determined via Ampères law

$$\mu_o\ j = \frac{1}{r}\ (r\ B_p)' \ . \tag{12}$$

From Eq. (12), making the usual assumption

$$j \simeq j_o \, (T_e/T_o)^{3/2} \quad , \tag{13}$$

with $T_e/T_o = 1 - r^2/a^2$ for simplicity, we obtain for B_p

$$B_p = \mu_o \, j_o \, a^2 \, \frac{1 - (1 - r^2/a^2)^{5/2}}{5r} \tag{14}$$

whence further

$$q \simeq \frac{2\pi \, B_o}{\mu_o \, IR} \, \frac{r^2}{1 - (1 - r^2/a^2)^{5/2}} \quad , \tag{15}$$

which is the expression for $q(r)$ we use in the code. At the plasma center, $r \rightarrow o$, we have

$$q(o) = 2 \times 10^6 Ba^2/RI, \tag{16}$$

whereas at the limiter, $q(a) = 2.5 \, q(0)$.

The remaining terms in Eqs (1) are defined as follows. P_{ohm} is the standard ohmic heating term. Its contribution to the power balance in the reactor configuration can be neglected. P_α is the Maxwellian α-particle energy production rate, approximated up to 100 keV by[20]

$$P_\alpha = \frac{4.29 \times 10^8 \, n^2 \exp(- 17.7/T_i^{0.348})}{1 - 0.05 \, T_i + T_i^{1/3} \, (0.1554 - 0.1418 \, T^{1/3} + 0.0364 \, T_i)} \quad . \tag{17}$$

The functions $f_{e,i}$,

$$f_e = \exp(- 0.015 T_e) \; , \; f_i = 1 - f_e \tag{18}$$

approximate the curves obtained in Ref. 21 for the fraction of α-particle energy going to the electrons and ions, respectively. We are assuming here that the α-particles deposit their energy locally, i.e. on the magnetic surface they were born, an approximation which improves with increasing plasma current and aspect ratio[11, 12]. Accounting for non-local deposition would widen the P_α heating profile; for 3.5 MeV particles and RFDTR parameters the banana orbit width is about 0.15 m, not a large effect on the scale of the given minor radius. The power P_{rad} radiated out of the plasma volume is principally composed of Bremsstrahlung P_{br} and impurity line radiation P_ℓ; we neglect synchrotron radiation. For Bremsstrahlung[19]

$$P_{br} = 5.35 \times 10^3 \, n^2 \, Z_{eff} \, T_e^{\frac{1}{2}} \quad , \tag{19}$$

and for P_ℓ we use the polynomial approximation[22]

$$P_\ell = 10^{27} \, n_I \, n \, L \quad , \tag{20}$$

where n_I is the impurity density, assumed radially to follow the profile $n(r)$, and

$$\log_{10} L = \sum_{i=0}^{5} A_i \, (\log_{10} T_e)^i \tag{21}$$

The coefficients A_i for elements up to Z = 90 are given in Ref. 22. Out of the large variety of high-Z impurity ions which might be present in a fusion-type tokamak discharge[23] we select Molybdenum to represent the whole group, noting that the dependence on T_e of P_ℓ for most of these elements has the same tendency to decrease with temperature between 1 and 10 keV. The coefficients A_i for Molybdenum are given in Table 2.

The energy equipartition term P_{eq} with a deuterium mass ratio ($m_i/m_e = 3600$) is[19]

$$P_{eq} = 26\ \nu_{ei}\ n\ (T_e - T_i) \quad , \tag{22}$$

where ν_{ei} is given by Eq. (9).

Finally, P_h represents supplementary heating,

$$P_h = \frac{P_{TOT}}{2\pi^2\ R\ a^2}\ C(T)\ h(r) \quad , \tag{23}$$

where P_{TOT} is the total available power (P_{TOT} = 100 MW for the purpose of this study), C(T) is a temperature-dependent control term and h(r) gives the spatial distribution of RF power deposition. As regards the control term, we may require, depending on the suitable diagnostic tool selected for monitoring T, that $C = C(T_e)$, for example. It is convenient to control as a function of one single parameter, however, and therefore we require that C be a function of peak (or average) temperature. The measurement of such a quantity can be performed on a very short time scale ($\simeq\mu s$), using X-ray spectrocopy, for instance. In order to achieve stable high-Q operation, given a steady operating density n_o, the control function C (T) must act to continuously decrease P_h as T approaches the point of ignition T_{ign} where thermal instability occurs.

The stability problem is discussed in some detail in the next section. We will require the function C (T) to remain constant up to near the projected operating temperature T_{op}, and then decrease as T approaches T_{ign}. A suitable representation is

$$C(T_{eo}) = \frac{1}{1 + \exp[\alpha_c(T_{eo} - T_{op})]} \tag{24}$$

where α_c is the rate of control. The coupling function h(r) in Eq. (23) is simplified to the extent that we suppress its possible explicit dependence on T_e, T_i, n, and on wave characteristics such as wave-guide configuration and the wave-number spectrum. A suitable representation for h(r) is

$$h(r) = \frac{1}{1 + \exp[-\alpha_h (r - r_h)]} \quad , \tag{25}$$

where r_h defines the extent of the heating region, and we take $\alpha_h = 10$ for rapid attenuation.

In order to test the performance of our heat transport model, Eqs (1), we have computed, for the ALCATOR-A configuration (Table 1), the principal global heat transport characteristic, the energy confinement time τ_E, defined as

$$\tau_E = \frac{4.8 \times 10^4 \langle n(T_e + T_i)\rangle}{\langle P_{ohm} - P_{rad}\rangle} \quad , \tag{26}$$

where

$$\langle \ldots \rangle = \frac{2}{a^2} \int_0^a (\ldots)\, r\, dr. \tag{27}$$

Such a definition of τ_E is the computational counterpart to the confinement time as determined from the results of measurements[10] of n, T, the plasma current and the loop voltage. The computations are summarized in Fig. 1. The solid lines of Fig. 1a, labelled 1 and 2, correspond, respectively, to

$\kappa_e = 1$ and to the κ_e of Ref. 17 [given roughly by Eq. (6)]. The τ_E all lie within the region of experimental data[10] scattered around the dashed line. In order to appreciate the effect of the ion-neoclassical contribution, we have included some results obtained with both enhanced and reduced κ_i. The crosses in Fig. 1 correspond to $\kappa_i \longrightarrow 3\kappa_i$, while the circles mark cases with a reduced $\kappa_i \longrightarrow \kappa_i/3$.

3 THERMAL STABILITY CRITERIA

We will discuss thermal stability criteria within the confines of a one-temperature representation of Eqs. (1a,b),an approximation which is valid when energy equipartition takes place on shorter time scale than the energy confinement time. In the range of parameters of interest here this is always true. We are then dealing with a single transport equation, nonlinear with respect to its state variable, the temperature. Such a system can possess several equilibria, characterized by distinct values of the temperature. An equilibrium of such a system is termed thermally unstable if its pertubation will result in the transition to another equilibrium state. The low-temperature ignition equilibrium of α-particle heated tokamaks (defined by that value of temperature at fixed density, magnetic field, etc. for which all losses are compensated by α-particle heating alone) is known to be thermally unstable. Some form of control is therefore required. Contributing to the power balance of a fusion plasma are power terms which are generally strongly radially nonuniform, as well as nonlinear in T. Such a term is, for example, the α-particle heating term P_α. To activate P_α, supplementary heating is required, itself possibly nonuniform in space, and nonlinear by virtue of the control term (24). If the effect of impurity line radiation is included, serious complications can arise on account of the fact that the radiative cooling rate increases with decreasing temperature. It can therefore be expected that radial nonuniformities will play an important rôle in the estab-

lishment of equilibrium, and of its thermal stability. Accordingly, under such conditions, a 1-D stability criterion is required for a reliable prediction of system operation. Ideally, one would like to understand the stability with respect to large perturbations from equilibrium, but no general method exists to date for nonlinear partial differential equations. Rather, we must content ourselves with the examination of stability with respect to small perturbations. For diffusion-type equations, the limited stability problem was solved by Gelfand[6]. We refer to Refs. 6, 7 and 8 for details. The essence of the Gelfand method is as follows. In order to determine the stability of the equilibria of the nonlinear equation

$$\frac{\partial T}{\partial t} = \frac{1}{r} \frac{\partial}{\partial r} \left[r \kappa(T, r) \frac{\partial T}{\partial r} \right] + S(T, r) = 0 \quad , \tag{28}$$

defined for r between r = 0 and r = a, and subject to the boundary conditions

$$T'(o) = 0 \ , \ T(a) = 0 \quad , \tag{29}$$

one has to first construct the plot of the radius a versus T_o, T_o being the value at the origin, of the solution of the equation

$$\frac{1}{r} \frac{d}{dr} \left(r \kappa \frac{dT}{dr} \right) + S(T, r) = 0 \ , \tag{30}$$

satisfying the conditions (29). Obviously, one does not have to solve a two-point boundary-value problem; if for a given T_o with $T'_o = 0$ the solution vanishes at some value of a, then this particular pair (T_o, a) constitutes an eigenpair. If for a T_o such a value of a does not exist,

then there are no equilibria for that particular T_o. The eigenfunctions for which the function $a(T_o)$ increases are stable, whereas those for which $a(T_o)$ decreases are unstable. Local minima and maxima of the function $a(T_o)$ mark points that are marginally stable. Singularities, i.e. points where $a(T_o)$ diverges, limit domains of existence of equilibria.

In most cases of practical interest, the $a(T_o)$ plot must be determined numerically. One proceeds as follows. First, a 0-D analysis gives a rough idea about the definition domain of the function $a(T_o)$. Then one integrates for a given T_o until either T drops below a certain reference noise level, or until T' changes sign in which case an equilibrium does not exist. Sometimes one is interested in the stability of equilibria in parameter spaces other than (T_o, a). Specifically, in our case of interest, fusion plasmas, the more relevant representation is in temperature - density space (T_o, n_o), for some specific, given, value of a. The determination of such a plot requires the scanning for a = const of many (T_o, a) plots produced at fixed n_o.

We now present, for the sake of comparison, the 0-D stability criteria. In (T_o, a) space we obtain a formally identical counterpart of the 1-D Gelfand criterion. The 0-D representation of Eq. (28) is obtained by assuming for T some reasonable form representing the quarterwave-like eigenfunction it should be, and subsequently integrating term by term over the given volume. The diffusion term, by application of Gauss' Theorem, becomes the rate of flow across the boundary. Hence, what we obtain amounts to a global energy conservation statement, in the general form

$$\frac{dT_o}{dt} = F(T_o;\ a,\ n_o,\ \ldots) \quad , \tag{31}$$

where the parameters a, n_o, and possibly others we have suppressed, are now all, mathematically speaking, equivalent. For a fixed set of parameters, an equilibrium T_{eq} of Eq. (31), defined as $F(T_{eq};\ a,\ n_o) = 0$, is stable with respect to small perturbation if and only if

$$\left.\frac{\partial F}{\partial T_o}\right|_{T_{eq}} < 0 \ , \tag{32}$$

as immediately follows from Eq. (31) upon varying T_o around T_{eq}. If we wish to express the stability condition (32) in parameter space $(T_o,\ a)$, for example, we note that,

$$\left.\frac{da}{dT_o}\right|_{F=0} = -\left.\frac{\partial F/\partial T_o}{\partial F/\partial a}\right|_{F=0} \tag{33}$$

The principal geometry effect in Eq. (31) originates in the diffusion term of Eq. (28). Hence the function F contains a term which scales as $-T_o/a^2$. Consequently $\partial F/\partial a > 0$, so that the equilibria are stable or unstable according to whether da/dT_o is positive or negative, respectively. Recalling the Gelfand criterion, we note that the two are identical; the only difference between the two cases is to be found in the actual location of the equilibria in parameter space. In contrast to 1-D, the paramter a in 0-D has no exclusive position on numerical or other grounds, so that we might as well go to the more useful $(T_o,\ n_o)$ representation. The equilibria in $(T_o,\ n_o)$ space are stable if and only if

$$\frac{dn_o}{dT_o}\,\frac{\partial F}{\partial n_o}\bigg|_{F=0} > 0 \quad . \tag{34}$$

Unlike $\partial F/\partial a$, the function (of T_o) $\partial F/\partial n_o$ is not necessarily definite in sign.

4 STABLE SUB-IGNITED EQUILIBRIA

In this section, we demonstrate the existence of stable sub-ignited equilibria of the system (1a, b), sustained by a temperature-controlled supplementary heating source. First, we give a rough picture of the equilibria and their stability in the presence of the controlled supplementary heating source using the 0-D approximation. More definite results are then obtained using the Gelfand method. Finally, we demonstrate heating and stable operation with the 1-D transport code. The 1-D simulations give us an opportunity to observe phenomena like instability with respect to large perturbations of the equilibria, and also temperature-profile collapse due to impurity radiation.

As a basis for the 0-D approximation as well as for the Gelfand method, we use a one-temperature model with a fixed (parabolic) density profile, as in the previous section. The two equations (1a, b), where we now neglect P_{ohm}, add up to

$$4.8 \times 10^4 \frac{\partial nT}{\partial t} = 1.6 \times 10^4 \frac{1}{r} [r(Q_e + Q_i)]' + P_\alpha + P_h - P_{rad} \quad , \qquad (35)$$

which, upon volume-averaging, gives the 0-D equilibria

$$F = \langle P_h \rangle - P_{diff} + n_o^2 \langle p_\alpha - p_{rad} \rangle = 0 \quad . \qquad (36)$$

The diffusion plus convection heat loss term can be written in the form

$$P_{diff} \simeq 4.8 \times 10^4 \frac{n_o T_o}{\alpha_p \tau_E} \quad , \qquad (37)$$

where $\alpha_p > 1$ is a profile factor and τ_E is the energy confinement time (5). In performing the volume-averages one must make some assumption about the profiles. Having already fixed the density profile, we assume, for the sake of simplicity of this rough model, a Gaussian temperature profile, $T = T_o \exp(-2r^2/a^2)$. Since $\tau_E \sim a^2 n_o$, we first note that the equilibria (36) can be written in the form

$$n_o^2 = \frac{P_{diff} - \langle P_h \rangle}{\langle p_\alpha - p_{rad} \rangle} = f(T_o), \qquad (38)$$

and that, second, $\partial F/\partial n_o$ is positive or negative depending on whether $\langle p_\alpha - p_{rad} \rangle$ is, respectively, positive or negative. The temperature for which $\partial F/\partial n_o = 0$ is thus the ideal ignition temperatude T_{id}. Recalling now the stability criterion (34), we see that the stable branches of the function (38) are those which for $T_o < T_{id}$ are decreasing, but increasing for $T_o > T_{id}$. As a first example, in Fig. 4a, of insufficient heating, we have applied a total power of 40 MW. If we initiate the system at a point lying anywhere below the upper branch of the $P_h > 0$ curve, the system will tend toward the lower, stable branch. For example, if the system is heated at constant density $n_o = 2$, starting at $T_e = 1$ keV, it will terminate at $T_o = 3.5$. Points lying above the upper $P_h > 0$ branch are all unstable (but inaccessible for the given P_h).

In Fig. 4b, we have increased P_{TOT} to 100 MW and in the control function C(T) of P_h, Eq. (35), we select $\alpha = 3$ and $T_{op} = 9$. The choice of T_{op} is basically determined by the position of the ignition curve. One could turn down the source at a higher value of T_{op}, but that would obviously be at the expense of having to operate a lower density in order not to risk runaway.

The optimum combination of T_{op} and of an operational density n_{op} would maximize thermonuclear yield but leave a sufficient safety margin of the operational point (T_{op}, n_{op}) against fluctuations that could carry the system over the ignition curve. In other words, defining the reactor Q-factor

$$Q = \frac{\text{power out}}{\text{power in}} = \frac{5 \langle P_\alpha \rangle}{\langle P_h \rangle} \tag{39}$$

one should aim for operating points having a high Q, keeping in mind the trade-off in terms of stability again fluctuations whose margin $\sim 1/Q$. Let us now return to Fig. 4b. The heating now amply compensates for losses in the region $T_o < T_{id}$ with the result that the system will heat at any density below $n_o = 10$. If, however, n_o exceeds 4 the system will heat indefinitely, having access to the unstable region beyond the ignition curve. A safe operating density for the controlled source would therefore be $n_{op} = 3$, for example, but only $n_{op} = 1$ for the uncontrolled case. The difference represents more than a factor of 10 in terms of thermonuclear yield. This is the principal raison d'être for the implementation of a controlled source. Going to higher values of power does not appreciably change the operating conditions for the controlled source. For an uncontrolled source, however, the equilibria shift to the right with increasing P_h, as follows from Eq. (38).

In principle then, stable operation is possible without control, but at the expense of Q, since the operating point on the slope of the uncontrolled source equilibrium curve is sustained at full power (which has to be increased if we desire a higher-temperature operating point) and low density. Thus, for the given example of $P_{TOT} = 100$ MW, the controlled Q is about 10

while, without control, $Q \simeq 1$. Higher values of Q can be attained in the 10 keV operating range, and without narrowing of the stability margin, if we include the effect of impurity line radiation. We are not suggesting, however, that the impurity level be artificially increased in order to achieve this, since other, deleterious, effects by far outweigh the benefit in terms of control and output at 10 keV. Specifically, as shown in Fig. 3 for a concentration of 10^{-4} n of Molybdenum the level of line radiation at 1 keV is higher by an order of magnitude than the level at 10 keV. The net result, shown in Fig. 2c, is that while the ignition curve shifts to the right, and slightly upward in the 10 keV region, the domain of densities for which the plasma will heat in the low-temperature region has substantially narrowed(and also the rate of heating will go down). Other effects of line radiation, not evident in 0-D, will be shown later.

The 0-D n_o versus T_o plots such as in Fig. 2 are easy to produce and serve as a useful guideline for locating the equilibria together with their stability properties, but a verification of stability of specific operating conditions is required and this is where the Gelfand method can be used. We show, in Fig. 4a, a versus T_o plots computed from the one-temperature model (35) under the conditions of Fig. 2b with a controlled source, for five values of n_o ranging from 1 through 5. Thus, for the configuration in question, i.e. for a minor radius a = 1.4 m, stable equilibria exist for $n_o \leq 2$. For $n_o > 3$ no equilibria exist at all. A more useful repre-sensation of the information contained in the a versus T_o plots parameterized with respect to n_o, are the loci of equilibrium points (T_o, n_o) for a given configuration (i.e. at fixed a) such as shown in Fig. 4b. To produce this plot

we first computed arrays of a versus T_o at fixed values of n_o (with steps of $\Delta T_o = 0.2$ and $\Delta n = 0.1$) and then selected all the data points (T_o, n_o) which fall into a certain interval centered around the given configuration value of a, i.e. around a = 1.4 in this particular case . For Fig. 4b, $1.3 \leq a \leq 1.5$. The lower boundary of the data point field corresponds to the upper bound of the a-interval, the upper boundary to the lower bound, i.e. to a = 1.3. The stable equilibria form the increasing branch of the n_o versus T_o curve, centered around T_o = 10 keV, as dictated by the control term. The total reactor output P_{out},

$$P_{out} \simeq 4\pi^2 R \int_0^a r dr \, 5P_\alpha \, , \tag{40}$$

corresponding to these stable equilibria is shown in Fig. 4c.

Let us now see how the preceding predictions fare in 1-D simulations of the system, Eqs. (1a, b) under conditions of Fig. 4. In these calculations we monitor the temperatures, the rate of change of the temperatures and the various power density terms. We terminate the computation if either dT/dt converges to zero, or if T_{io} exceeds a certain limit, in which case we know that control has failed. The results for the given case of wide-profile heating ($r_h = 1$) are that for $n_o = 2$ the system stabilizes at T_{io} = 9.5 keV, while at n_o = 3 and 4, runaway occurs. In Figs. 5 a, b, c we show, for illustration, the profiles of temperature, density, of the heating terms P_α and P_h (all at the end of the run), and the time evolution of T_i, in the unstable case of $n_o = 3$. While instability was expected at $n_o = 4$, the failure of the system to stabilize at $n_o = 3$ is most likely due to a large perturbation effect of the heating source P_h.

To understand this we recall that the Gelfand stability criterion holds true for small perturbations of the equilibria. In the case of bulk plasma heating, before equilibrium is reached, the P_h term is not only larger in magnitude , but also has a wider radial profile then the P_α term. The corresponding temperature profile thus approaches equilibrium in a state which is, in fact, strongly perturbed with respect to the equilibrium temperature profile, sustained at (presumably) high-Q operation principally by P_α. Since the system is perturbed in the direction of a larger energy content, it will have the tendency to run away once it approaches the marginal stability boundary. We have observed the same effect when the system was initialized with a wide temperature profile near the marginal stability boundary. If, in contrast, the supplementary heating term P_h is made to have a radial profile which is narrower than the P_α term, there should be no danger of runaway even in the region of marginal stability. An example of such plasma core heating is shown in Fig. 6. Here, all the available heating power is concentrated within a radius of $r_h = 0.35$ m (rather than within $r_h = 1$ as was the case in Fig. 5). We observe that for a peak density of $n_o = 4$ the system first relaxes at equilibrium but ultimately runs away, while at $n_o = 3$ we have stable operation. We thus conclude that core heating is a thermally more stable process than bulk heating (in addition to being faster and more efficient). It appears strange, of course, that core heating, associated as it is with high power densities, does not cause runaway more easily than does bulk heating. It is useful to keep in mind, in regard to this question, that the heating source is directly temperature-controlled. If it weren't, bulk heating would, in fact, be the less unstable heating process.

In what follows, we briefly examine the effect, on thermal stability, of a nonuniform heat conductivity and of impurity line radiation. So far, we have postulated that the dominant heat transport process, anomalous electron heat conduction, can be represented by a constant heat conductivity, $\kappa_e \simeq 10^{20}\ m^{-1}s^{-1}$, compatible with empirical scaling for the energy confinement time. On the other hand, the ion-neoclassical contribution [Eqs. (3) and (4)] is nonuniform and nonlinear. In terms of magnitude, the conductivity κ_i is (in the parameter range of interest) much smaller than κ_e everywhere except very near the plasma center. Thus although κ_i contributes very little to the global heat loss, it can have an important local effect in the plasma core. This can be appreciated particularly in the case of plasma core heating, since a centrally peaked conductivity enhances the rate of heat flow away from the region of high power densities. Such an enhancement can have a stabilizing or destabilizing effect depending on the state of the system. The examples of Fig. 7 will help to clarify this point. In Fig. 7a, the conductivity is taken as $\kappa = \kappa_e + 5\ \kappa_i$ in order to amplify the nonuniform contribution. In contrast, Fig. 7b has $\kappa = \kappa_e$, i.e. the nonuniform contribution is suppressed. The system equilibria are slightly different in the two cases, and so is their stability. The uncontrolled (ignition) equilibria are more stable, as one would expect, when $\kappa = \kappa_e + 5\ \kappa_i$. In contrast, the controlled equilibria around $T_o = 10$ are more stable when κ_i is suppressed! This result, which appears to contradict standard notions about the effect of enhanced loss on stability is, however, perfectly understandable. With the contribution of the centrally peaked ion conductivity gove, less energy is flowing away from the center and since the peak temperature itself is controlled, the

only effect of such a peaked conductivity is to produce a narrower and thus more stable, temperature profile. We thus conclude that in the presence of control the ion-neoclassical contribution has a destabilizing effect, while in the absence of control or in a nonequilibrium situation, a centrally peaked conductivity will have a stabilizing effect.

The heat conductivity is not only nonuniform but also is nonlinear. In the case of κ_i the two effects are, in fact, coupled. In the plasma core, specifically, the principal radial dependence of κ_i is implicit, via the $T^{3/2}$ factor. The preceding conclusions, with regard to stability, are of course generally true for any centrally peaked conductivity, but for the particular case in question, the nonlinearity acts to enhance those features, because an upward fluctuation in temperature will cause an upward fluctuation in conductivity.

To close this section, we briefly touch upon some difficulties due to line radiation associated with the presence in the plasma of high-Z impurities, namely of Molybdenum, selected to represent this group of elements. We will consider the effect of an impurity concentration $n_I = 10^{-4}$ n, an amount which is still tolerable from a global energetics point of view (Fig. 3). To observe a discernable effect in the high-temperature region a much more serious effect could therefore be expected at low temperatures. For example, as is well known, much more supplementary power would be required. Apart from this fact though, even in the apparently "safe" domain of around $n_I \simeq 10^{-4}$ n, more subtle, 1-D effects, can upset an equilibrium. In the case of core heating, for example, an effect which we term a "contraction instability"

can occur. We show in Fig. 8 the result of a 1-D simulation, under the conditions of Fig. 6, but with line radiation. The equilibrium is now perfectly stable, as is evident from Fig. 8a, but the temperature profile shown in Fig. 8b has shrunk to about half its normal width, intolerably reducing as a consequence the power output. What causes the contraction is that once the temperature is allowed to decrease as a result of line radiation, the rate of radiation increases, followed by a further drop in temperature, and so on. The process will penetrate inward until the power loss is compensated by heat flowing down the gradient or by the supplementary heating directly. Thus, in the presence of line radiation, heating of the bulk of the plasma is probably a better stratagem than heating only of the core, although even then difficulties may arise. We take again the conditions of Fig. 8, only now with $r_h = 1$. The result, shown in Fig. 8c, exhibits a tendency of the profile to invert, for the same reason why it contracts in the preceding example. The inversion, in this example, however stops at a certain instant in time and the profile gradually recovers. To sum up then, the presence of impurities is likely to obstruct optimum heating strategy wherein less total power could be used to preferentially heat the plasma core.

5 REALIZATION OF REACTOR CONFIGURATION

So far we have demonstrated heating and control, and discussed a number of radial effects, without the consideration of optimizing the reactor output. If we go back to Fig. 4, we note that the total output at $T_{op} = 10$ and $n_o = 3$ is about 440 MW. This number, obtained with transport coefficients corresponding to empirical ALCATOR-A scaling, falls short of what is generally expected in terms of output from a configuration of this size, at the given operating conditions. More specifically, the power outputs quoted[24] for configurations of the type of UWMAK, HFCTR and STARFIRE are all between 2 000 and 4 000 MW thermal, numbers which are reasonably high for a viable power plant. If we examine the origin of the discrepancy between our result and the projected system outputs, we conclude that the latter must have assumed almost flat density and temperature profiles. If, for example, we take a uniform plasma at T = 10 keV and $n = 3 \times 10^{20}$ m^{-3}, occupying a volume of 300 m^3, we obtain a total power output of 1 750 MW. If we increase the operating temperature to 15 keV, say, the output approximately doubles. When, however, profile effects are taken into account, the output must be reduced by about a factor of 4, in the case of a parabolic density and temperature. It is not difficult to see that the dominant profile effect is caused by the temperature on account of the P_α term, which is a strongly nonlinear and increasing function of T (Fig. 3). Any system studies which fail to correlate the power output to a specific temperature profile are therefore unrealistic. Equally unrealistic are hopes that more rigorous assessments, based on transport codes with scaled-up configurations using present-day transport coefficients, as in the example

of Fig. 4, will produce interesting outputs.

We have, therefore, asked ourselves the question what assumptions must be made about heat transport in order to obtain an output of about 2 000 MW, at sub-ignited stable operation. Our task is, in effect, more difficult than just a straightforward attempt to increase the output, since the system stability deteriorates with increased output. Let us begin with a 0-D discussion. At a presumed high-Q equilibrium, P_h in Eq. (36) can be neglected, and so can P_{rad}; the diffusion heat loss is balanced by α-production. The total power output (40) can therefore be estimated as

$$P_{out} \simeq 2.4 \times 10^5 \frac{n_o T_o}{\alpha_p \tau_E} 2\pi R a^2 , \qquad (41)$$

where $\alpha_p > 1$ is a profile factor. For the conditions of Fig. 4, and with $\alpha_p \simeq 4$, the approximation (41) gives $P_{out} \simeq 400$ MW, compatible with the transport code result. There is, however, not much one can do to increase P_{out}. First of all, we are restricted in our choice of peak operating density and temperature by β, and thermal stability conditions, and second, if $\tau_E \sim a^2$ then P_{out} does not depend on the minor radius. Let us therefore examine to what extent do α_p and τ_E depend on the heat conductivities. A radially uniform increase of the total heat conductivity cannot affect α_p but $\tau_E \sim a^2/\kappa$, so that P_{out} increases in proportion. The thermal stability of a fixed operating point T_o, n_o below ignition improves with decreasing τ_E, since, as a result, the ignition curve moves upward in the (T_o, n_o) plane. Nonuniform changes in the heat conductivity will

affect the temperature profiles. Let us consider, specifically, an enhancement which decreases with radial position. This is the case when, for example, the ion-neoclassical conductivity is increased by a constant factor, or if we replace the constant anomalous electron conductivity by an expression of the type (6). The global effect of such a variation in κ is difficult to assess, but if κ increases principally in the plasma core, not much of a change in τ_E can be expected. However, there can be an appreciable widening of the temperature profile, with a corresponding decrease in the value of α_p. Again, the power increases, but the configuration becomes less stable, as is clear from the results of the previous section. A few examples will help to clarify the preceding discussion.

In the example of Fig. 8 we keep the configuration of Fig. 4, the only change being a higher $T_{op} = 15$, and a wider density profile, $n = n_o \exp(-r^2/a^2)$. As expected, the output has increased but is nowhere near our goal of 2 000 MW. In all of the following examples we take $T_{op} = 15$ keV and a parabolic density profile, but we increase, one way or another, the total heat conductivity. As a first step, we increase the ion-neoclassical coefficient κ_i by a factor of five, in accord with current ideas[25] about enhanced ion-neoclassical transport [to explain the observed deviation at high plasma densities of the energy confinement time from the so-called ALCATOR-scaling (5)]. This enhancement itself proves insufficient to appreciably influence the power output, simply because the ion-neoclassical contribution is small compared to the electron anomalous effect in the first place. The temperature profiles, however, widen some-

what and we, therefore, retain the fivefold neoclassical enhancement in the next examples, where the electron anomalous effect is also enhanced.

With a further enhancement of loss it becomes difficult to heat the plasma with only 100 MW of supplementary power. In addition, wall loading becomes a problem. In the following last two examples we therefore increase the minor radius from a = 1.4 m to a = 2 m (and I from 3MA to 6MA to maintain the value of q). We recall that P_{out} will not change as a result of such a modification, but it becomes easier to heat the plasma before P_α is sufficiently large. Figure 10 shows the result of a simple upscaling of κ_e by a factor of three (from the value κ_e = 1 compatible with empirical scaling). As expected, the output (Fig. 10b) increased by about a factor of three compared to the case of κ_e = 1 in Fig. 4c. In order to introduce a profile effect to push up P_{out}, we now take the theory-based anomalous expression(6). Although the average value $\langle\kappa_e\rangle$ is still only about three, as in the previous example, the output is now larger, due to a wider temperature profile. The associated n_o versus T_o Gelfand plot in Fig. 11a gives stable equilibria up to $T_o \simeq 16$ and $n_o \simeq 3.1$. The total output corresponding to these equilibria is shown in Fig. 11b. At n_o = 3, T_o would be 15.5 keV (from Fig. 11a), with an output of about 2 000 MW. We have verified these results using the 1-D transport code. We show here, in Fig. 12, one particular simulation result, for n_o = 3.1, aimed principally at testing the stability boundary of Fig. 11a. First, in Fig. 12a we note the wide temperature profile (compared to that of

Fig. 5a.). Second, in Fig. 11b we see T_i slightly increasing as a function of time, as expected for a marginally unstable operating point. At $n_o = 3$, we obtained a perfectly steady equilibrium associated with a total output of 2 200 MW, and Q = 75. We also monitored the energy confinement time

$$\tau_e = \frac{4.8 \times 10^4 \langle n(T_e + T_i)\rangle}{\langle P_\alpha + P_h - P_{rad}\rangle} \quad . \tag{42}$$

In the example of Fig. 12, $\tau_E = 0.9$ s.

We thus conclude our effort to establish conditions under which a Tokamak reactor average power density of about 4 MW/m^3 can be realized during steady sub-ignited operation. While large values of the energy confinement time, τ_e, are beneficial in the heating phase, at equilibrium, in contrast, smaller values of τ_E (about 1s) are necessary for large power outputs and thermal stability. In addressing, ultimately, the question whether such heat transport properties can be expected to exist at reactor conditions, we recall that a number of present-day theory-based anomalous electron heat conductivities[17, 18, 26] exhibit the scaling $T^{\frac{1}{2}}$ having the necessary property. Unfortunately, while all these anomalous expressions give about the same numbers for present-day experiments, they differ by wide margins at reactor conditions. This is why we have extracted the common factor $T^{\frac{1}{2}}$ and suppressed the dependence on other parameters lumping them into a numerical coefficient consistent with empirical τ_e. Finally, in going from ohmically to RF-heated plasmas some deterioration of τ_E can be expected, but the experimental evidence so far[16] is too scarce to make any definite conclusions about the size of this effect.

6 SUMMARY AND CONCLUSION

We have demonstrated the existence of stable radial sub-ignited equilibria of a tokamak reactor, sustained in operation by a feedback-controlled supplementary heating source. The establishment of stability depends on a number of radially nonuniform processes whose effect we have attempted to analyse using both the Gelfand method and a 1-D fluid code.

Present-day tokamak experiments indicate the pre-eminence, in the tokamak power balance, of heat loss. In a reactor configuration we would expect an equally large proportion of power loss via diffusive and convective processes with at least an equally important share due to anomalous electron processes. We have therefore postulated the form of ALCATOR scaling for the energy confinement time, and, given the lack of a definitive theory of anomalous transport, we have assumed the simplest possible forms for the associated transport coefficients, consistent with both the empirical scaling law[10] and existing theory[17, 18, 25]. That is, we assume an enhanced neoclassical ion heat conductivity, an anomalous particle diffusion coefficient inversely proportional to density and an electron heat conductivity which is either constant or proportional to $T^{\frac{1}{2}}$. With such a choice of transport coefficients we avoid introducing arbitrary radial effects, attributing the principal nonuniformity in heat transport to neoclassical effects and to a theory-based $T^{\frac{1}{2}}$ scaling in the anomalous contribution.

The heat conductivities peak at the plasma center and there is, consequently a correspondingly high rate of heat flow away from the plasma core,

at the expense of α-particle heat production. Since this rate of flow decreases toward the plasma edge, the net effect is a wider temperature profile than one corresponding to a uniform or radially increasing flow. How do we understand this effect in terms of stability? We have to distinguish between a nonequilibrium and an equilibrium situation. In a nonequilibrium state during the heating phase, for instance, a large rate of flow away from the center has a stabilizing effect, strongly enhanced by the nonlinearity of κ with respect to temperature. Once an equilibrium is established, however, in a controlled fashion wherein the central temperature is kept constant, an upward local fluctuation in the rate of heat flow has a destabilizing effect, and vice versa. This is understood on the grounds that a local enhancement in the value of conductivity acts to extract more power from the α-particle heat bath, accumulating this excess power elsewhere in the plasma. A less stable configuration results. Similarly, a downward local fluctuation in heat conductivity results in a more stable equilibrium configuration as can be witnessed from the Gelfand plots in Fig. 7. In sum then, if a radially nonuniform and nonlinear heat conductivity tends to peak at the location of maximum heat production (typically the plasma core), there is a profound effect on the thermal stability of the configuration. Namely, an upward fluctuation in conductivity enhances stability when no control is implemented, while controlled equilibria become less stable in consequence.

Equally difficult to understand within the confines of a 0-D model are radial effects due to the supplementary heating. Equilibria resulting from various heating profiles can be adequately distinguished in 0-D; the

issue, however, is the nonequilibrium heating phase in the evolution of the temperature profiles. If heating is radially uniform, the non-equilibrium temperature profile tends to be much wider than its eventual equilibrium profile, corresponding at high-Q operation to predominantly α-particle heating, a term that is centrally strongly peaked. The system thus arrives at the anticipated controlled equilibrium in a strongly perturbed state and thermal runaway is likely to occur. It thus appears safer to aim for core heating (associated with narrower heating profiles) which is also the more advantageous stratagem as far as the rate of heating and total power requirements are concerned. Core heating is, however, not without problems of its own, and these are due to impurity line radiation.

Line radiation is again a term difficult to incorporate into a 0-D model. The reason now is that the radiated power density is a decreasing function of electron temperature, with the result that not only is the total radiated power large when least needed, i.e. when the average plasma temperature is low, but also, the radiative cooling rate tends to increase toward the plasma edge. As a result, when most of the supplementary power is concentrated into the plasma core, the temperature profile is susceptible to contraction, an instability driven by the uninhibited increase in the cooling rate as the temperature drops in consequence. We have observed this effect at low levels of high-Z impurity concentration (10^{-4} n of Molybdenum with a Gaussian density profile) and thus we conclude that the effect of contraction is likely to present a serious problem in thermonuclear plasmas which are not extremely clean.

To conclude our analysis, we have examined, both computationally and using a 1-D thermal stability criterion, the conditions necessary for achieving a tokamak reactor output of about 2 000 MW at steady, high-Q operation. Essentially, with an assumed parabolic density profile, for steady operation at a peak temperature of about 15 keV, one may not exceed a peak density of about 3×10^{20} m^{-3}. Given these restrictions, one then requires relatively wide (at least parabolic) temperature profiles and an energy confinement time not exceeding about 1 s. These requirements can be met if heat transport at reactor operating conditions is assumed to be determined by ion-neoclassical and theory-based ($\sim T^{\frac{1}{2}}$) electron-anomalous diffusion coefficients, both enhanced with respect to present-day theory values.

REFERENCES

1. International Tokamak Reactor INTOR: Zero Phase, IAEA, Vienna (1980), Chap. III.

2. Bromberg, L., Cohn, D.R., Williams, J.E.C., Compact Tokamak Ignition Reactors for Alpha Particle Heating and Burn Control Studies, MIT Plasma Fusion Center, Report RR-78-12 (1979).

3. Borrass, K., Gruber, O., Lackner, K., Minardi, E., Neuhauser, J., Wilhelm, R., Wunderlich, R., Bromberg, L., Cohn, D.R., Ignition and Burn Control in Tokamak Plasmas, Plasma Physics and Controlled Nuclear Fusion Research 1980, Paper IAEA-CN-38/W-2-1.

4. Bromberg, L., Fisher, J.L., Cohn, D.R., Nucl. Fusion 20, 203 (1980).

5. Harten, L. Fuchs, V., Bers, A., Nucl. Fusion 20, 833 (1980).

6. Gelfand, I.M., Amer. Math. Soc. Transl. (2), 29, 295 (1963).

7. Kolesnichenko, Y.I., Reznik, S.N., Yavorskij, V.A., Nucl. Fusion 16, 105 (1976); Kolesnichenko, Y.I., Reznik, S.N., Nucl. Fusion 18, 1535 (1978); Kolesnichenko, Y.I., Nucl. Fusion 20, 727 (1980).

8. Rosenau, P., The Physics of Fluids, 25, 148 (1982).

9. Cohn, D.R., Schultz, J.H., Bromberg, L., Chang, F., Cook, D.L. et al., High Field Compact Tokamak Reactor (HFCTR) Conceptual Design, MIT Plasma Fusion Center, Report RR-79-2 (1979).

10. Gondalekhar, A., Overskei, D., Parker, R., West, J., Energy Confinement in ALCATOR, MIT Plasma Fusion Center, Report RR-78-15 (1978).

11. Mc Allees, D.G., Alpha Particle Energetics and Neutral Beam Heating in Tokamak Plasmas, ORNL-TM-4661, Oak Ridge (1974).

12. Mikkelson, D.R., Post, D.E., A Parametric Study of Alpha-Particle Heating in Tokamaks in Physics of Plasmas in Thermonuclear Regimes, Proceedings of the 1979 Workshop, International School of Plasma Physics, Varenna, Italy (1979).

13. Düchs, D.F., Post, D.E., Rutherford, P.H., Nucl. Fusion 17, 565 (1977).

14. Ames, W.F., Numerical Methods for Partial Differential Equations, Barnes & Noble, N.Y. (1969).

15. Ahlberg, G.H., Nilson, E.N., Walsh, J.L., The Theory of Splines and Their Applications, Academic Press, N.Y. (1980).

16. Equipe TFR, ICRE Heating in TFR 600, Plasma Physics and Controlled Nuclear Fusion Research 1980, Paper IAEA-CN-38/D-3.

17. Molvig, K., Hirshman, S.P., Whitson, J.L., Phys. Rev. Lett. 43, 582 (1979).

18. Ohkawa, T., General Atomic, Report No. GA-A1-4433 (1977).

19. Spitzer, L. Jr., Physics of Fully Ionized Gases, Interscience Publishers, Chap. 5 (1962).

20. Galbraith, D.L., Kammash, T., The Dynamic Behavior of a Mirror Fusion Reactor, EPRI Report ER-521 (1978).

21. Sigmar, D.J., Joyce, G., Nucl. Fusion 11, 447 (1971).

22. Post, D.E., Jensen, R.V., Tarter, C.B., Grassberger, W.H., Lokke, W.A., Atomic Data and Nuclear Data Tables 20, 397 (1977).

23. Bhadra, D.K., IEEE Trans. Plasma Science Ps-9, 85 (1981).

24. Baker, C.C., Proceedings of the IEEE 69, 917 (1981).

25. Wolfe, S.M., Bull. Amer. Phys. Soc. 26, 918 (1981).

26. Cordey, J.G., Nucl. Fusion 20, 1617 (1980).

FIGURE CAPTIONS

Fig. 1 Code benchmarking. Energy confinement time, τ_E, versus average density, $\langle n \rangle$. The dashed line is the ALCATOR-A experimental result. The points lying on the curves 1, 2 are computed from Eq. (26). The curves 1 and 2 correspond, respectively, to $\kappa_e = 1$ and $\kappa_e = 1.5T_i^{\frac{1}{2}}$. The circles correspond to a threefold reduction, and the crosses to a threefold enhancement, of the ion-neoclassical conductivity.

Fig. 2 0-D equilibria in peak density, n_o, versus peak temperature, T_o, space. The ignition equilibria correspond to no supplementary heating, otherwise bulk heating is applied. Control implemented at $T_{op} = 9$. (a) Total applied supplementary power, $P_{TOT} = 40$ MW; line radiation $P_\ell = 0$. (b) $P_{TOT} = 100$ MW; $P_\ell = 0$. (c) $P_{TOT} = 100$ MW, $P_\ell \neq 0$ corresponding to a concentration of $10^{-4}n$ of Molybdenum.

Fig. 3 Power densities, P, versus temperature, T, for a uniform density $n = 1$. P_{diff} is the diffusion loss [Eq. (37)], P_{br} is Bremsstrahlung Eq. [(19)], P_{line} is line radiation [Eq. (20)], and P_α the heating rate due to α-particles [Eq. (17)].

Fig. 4 (a) Gelfand plots for Eq. (35). Radius, a, versus peak temperature, T_o, for 5 different values of peak density, n_o. Bulk heating, $P_{TOT} = 100$ MW, $P_\ell = 0$. (b) Corresponding n_o versus T_o equilibria for $1.3 \leq a \leq 1.5$. (c) Total reactor power output of the stable (increasing) branch in (c) as a function of peak density.

Fig. 5 1-D simulation [Eqs. (1)]. Bulk heating, P_{TOT} = 100 MW, $P_\ell = 0$, $n_o = 3.3$. (a) Density, n, and temperatures, T_e and T_i, as a function of radial distance, r, at $\tau = 3$ s. (b) Power source densities, ℓn P, as a function of radial distance, r. (c) Peak ion temperature, T_{io}, as a function of time, t.

Fig. 6 Core heating, $r_h = 0.35$ m, $T_{op} = 10$ keV, $P_{TOT} = 100$ MW, $P_\ell = 0$. (a) n_o versus T_o equilibria for $1.3 \leq a \leq 1.5$. (b) 1-D simulation; T_{io} versus time for $n_o = 3.1$.

Fig. 7 N_o versus T_o equilibria for $1.3 \leq a \leq 1.5$, $T_{op} = 10$; core heating, $P_{TOT} = 100$ MW, $P_\ell = 0$. (a) $\kappa = \kappa_\ell + 5\kappa_i$. (b) $\kappa = \kappa_e$.

Fig. 8 1-D simulation of core heating with line radiation corresponding to 10^{-4} n of Molybdenum. Otherwise conditions as in Fig. 6. (a) T_{io} versus time. (b) Equilibrium temperature profiles. (c) Nonequilibrium temperature profiles during bulk heating ($r_h = 1$ m).

Fig. 9 (a) n_o versus T_o equilibria for $T_{op} = 15$ keV, otherwise, conditions as in Fig. 6. (b) Corresponding total power output as a function of peak density.

Fig. 10 (a) n_o versus T_o equilibria for $T_{op} = 15$ keV, $1.9 \leq a \leq 2.1$, and enhanced heat conductivities $\kappa_e = 3$, $\kappa_i = 5\ \kappa_{neoclassical}$. (b) Corresponding total power output as a function of peak density.

Fig. 11 (a) n_o versus T_o equilibria under conditions of Fig. 10, except that $\kappa_e = 1.5\ T_i^{\frac{1}{2}}$. (b) Corresponding total power output as a function of peak density.

Fig. 12 1-D simulation under conditions of Fig. 11, for $n_o = 3.1$. (a) Temperature profiles at $\tau = 1.5$ s. (b) Peak ion temperature, T_{io}, as a function of time, τ.

Table 1

TOKAMAK CONFIGURATION PARAMETERS

	RFDTR	ALCATOR-A
Major radius, R	8 m	0.56
Minor radius, a	1.4 - 2 m	0.1
Toroidal field, B	6 T	6
Plasma Current, I	3 - 6 MA	0.2
Peak equilibrium Temperature, T_o	10 - 15 keV	0.5 - 1.2
Peak equilibrium Density, n_o	(1-4) x 10^{20} m^{-3}	1 - 10
Central safety factor, q_o	$\simeq$ 1	$\simeq$ 1
Heating	100 MW (RF)	Ohmic

Table 2

THE COEFFICIENTS A_i FOR THE DETERMINATION OF LINE RADIATION, EQS (20) AND (21), OF MOLYBDENUM

	0.08 - 0.2 keV	0.2 - 2 keV
A_0	- 139.1054	- 17.72591
A_1	- 649.3335	- 1.058217
A_2	- 1365.838	- 3.583172
A_3	- 1406.464	1.660089
A_4	- 708.6213	8.565372
A_5	- 140.0571	4.532909
	2 - 20 keV	20 - 100 keV
A_0	- 13.85096	39.92683
A_1	- 36.78452	- 175.7093
A_2	114.0587	207.4927
A_3	- 163.5634	- 121.4589
A_4	107.6260	35.31804
A_5	- 26.42488	- 4.083832

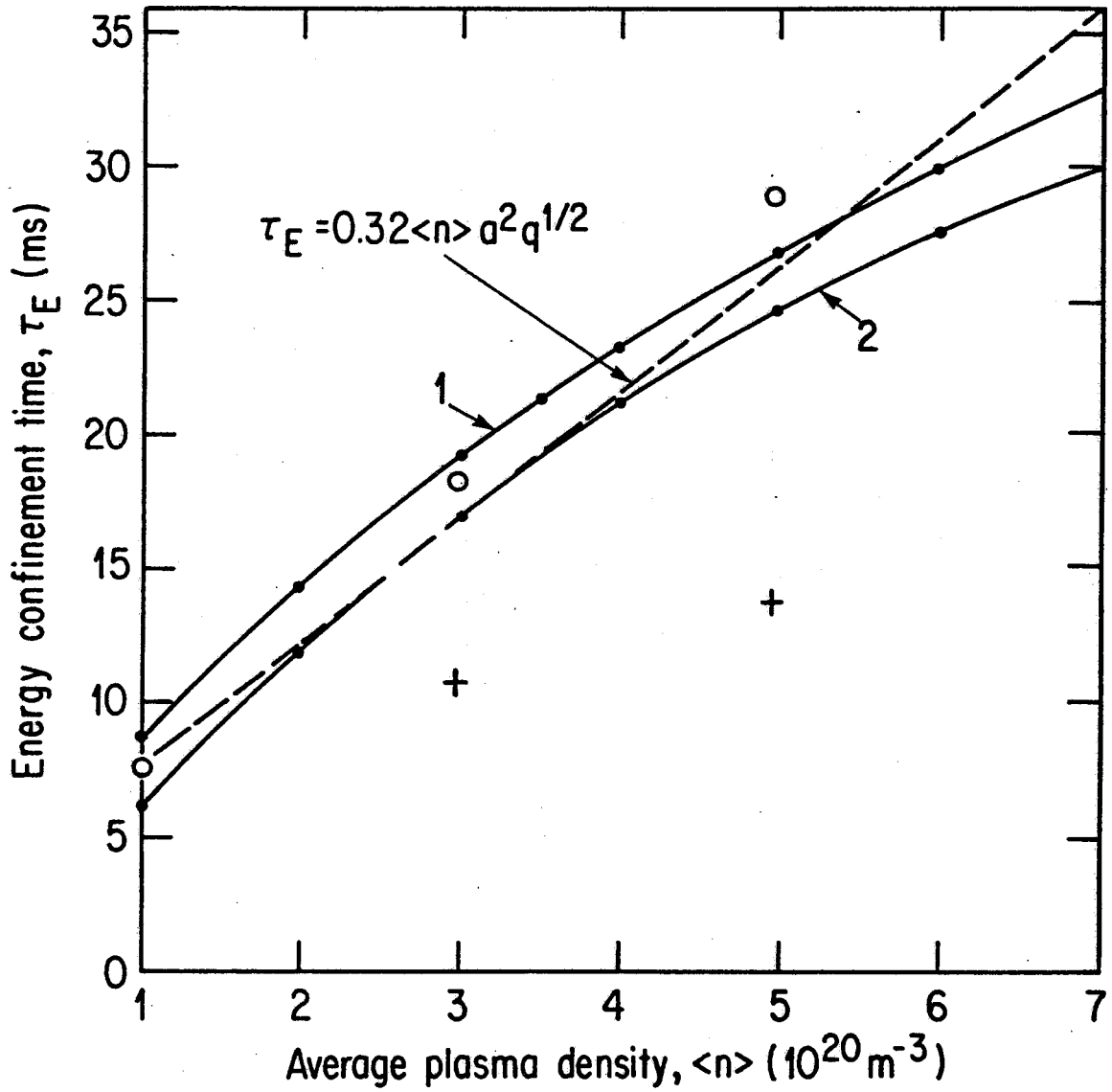
35
30
25
20
15
10
5
0
1
2
3
4
5
6
7
Energy confinement time, τ_E (ms)
Average plasma density, <n> (10^{20} m^{-3})
$\tau_E = 0.32 \langle n \rangle a^2 q^{1/2}$
1
2

Fig. 1

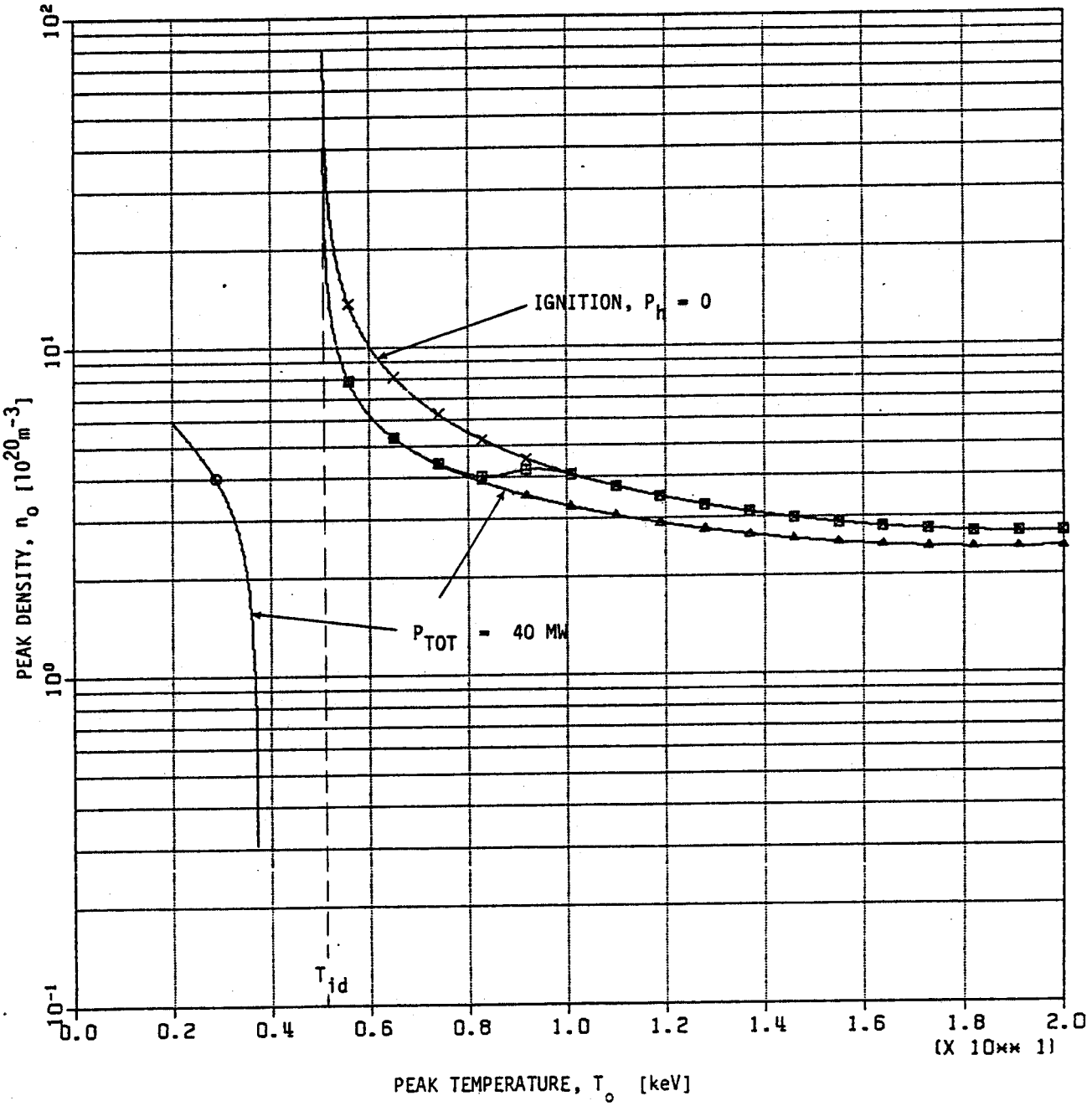
PEAK DENSITY, n_o [$10^{20}m^{-3}$]
10^2
10^1
10^0
10^{-1}
IGNITION, P_h = 0
P_{TOT} = 40 MW
T_{id}
0.0
0.2
0.4
0.6
0.8
1.0
1.2
1.4
1.6
1.8
2.0
(X 10** 1)
PEAK TEMPERATURE, T_o [keV]

Fig. 2a

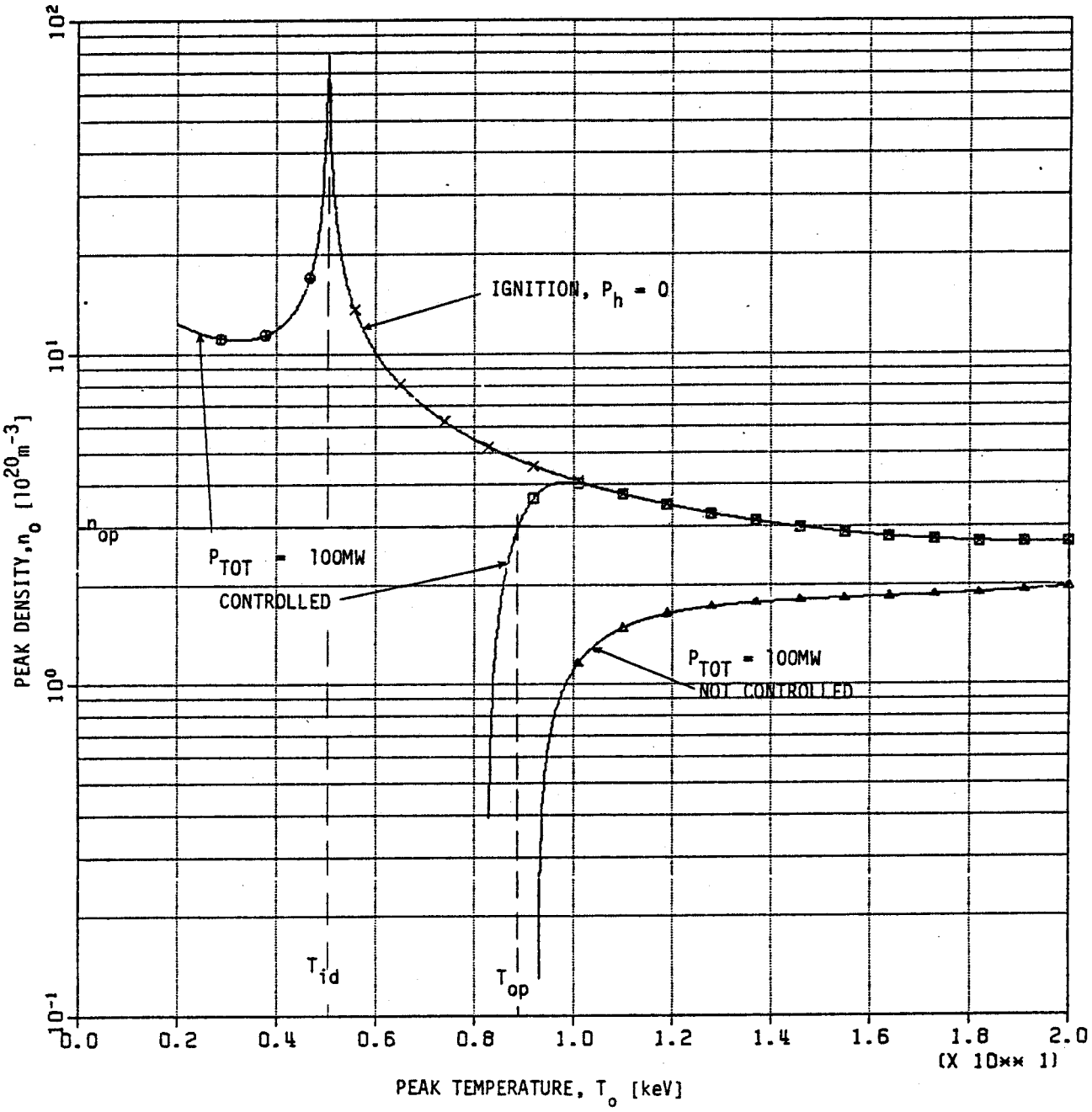
PEAK DENSITY, n_o [$10^{20} m^{-3}$]
10^2
10^1
10^0
10^{-1}
IGNITION, P_h = 0
n_{op}
P_{TOT} = 100MW
CONTROLLED
P_{TOT} = 100MW
NOT CONTROLLED
T_{id}
T_{op}
0.0
0.2
0.4
0.6
0.8
1.0
1.2
1.4
1.6
1.8
2.0
(X 10** 1)
PEAK TEMPERATURE, T_o [keV]

Fig. 2b

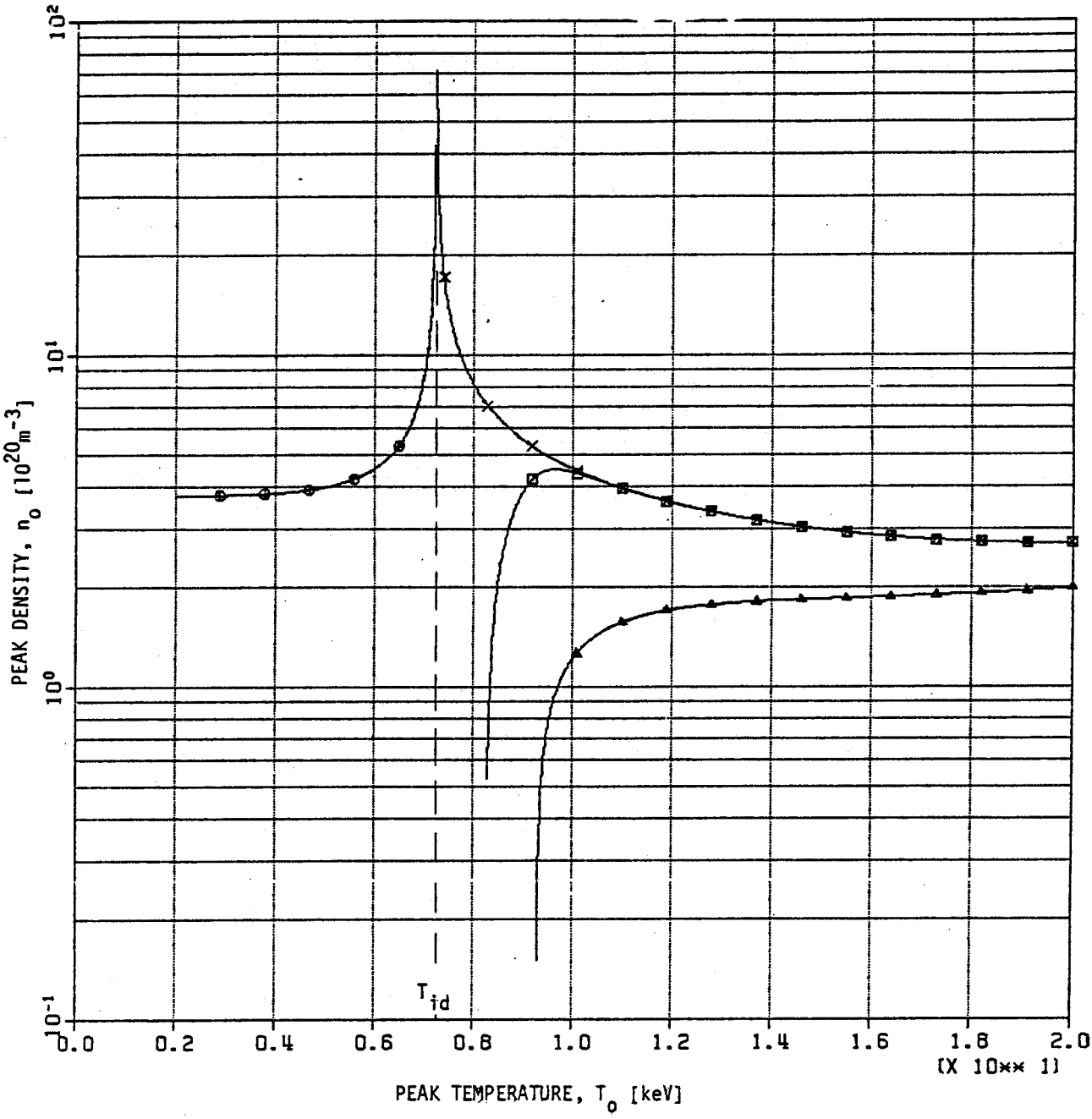
PEAK DENSITY, n_o [$10^{20}m^{-3}$]
10^2
10^1
10^0
10^{-1}
T_{id}
0.0
0.2
0.4
0.6
0.8
1.0
1.2
1.4
1.6
1.8
2.0
(X 10** 1)
PEAK TEMPERATURE, T_o [keV]

Fig. 2c

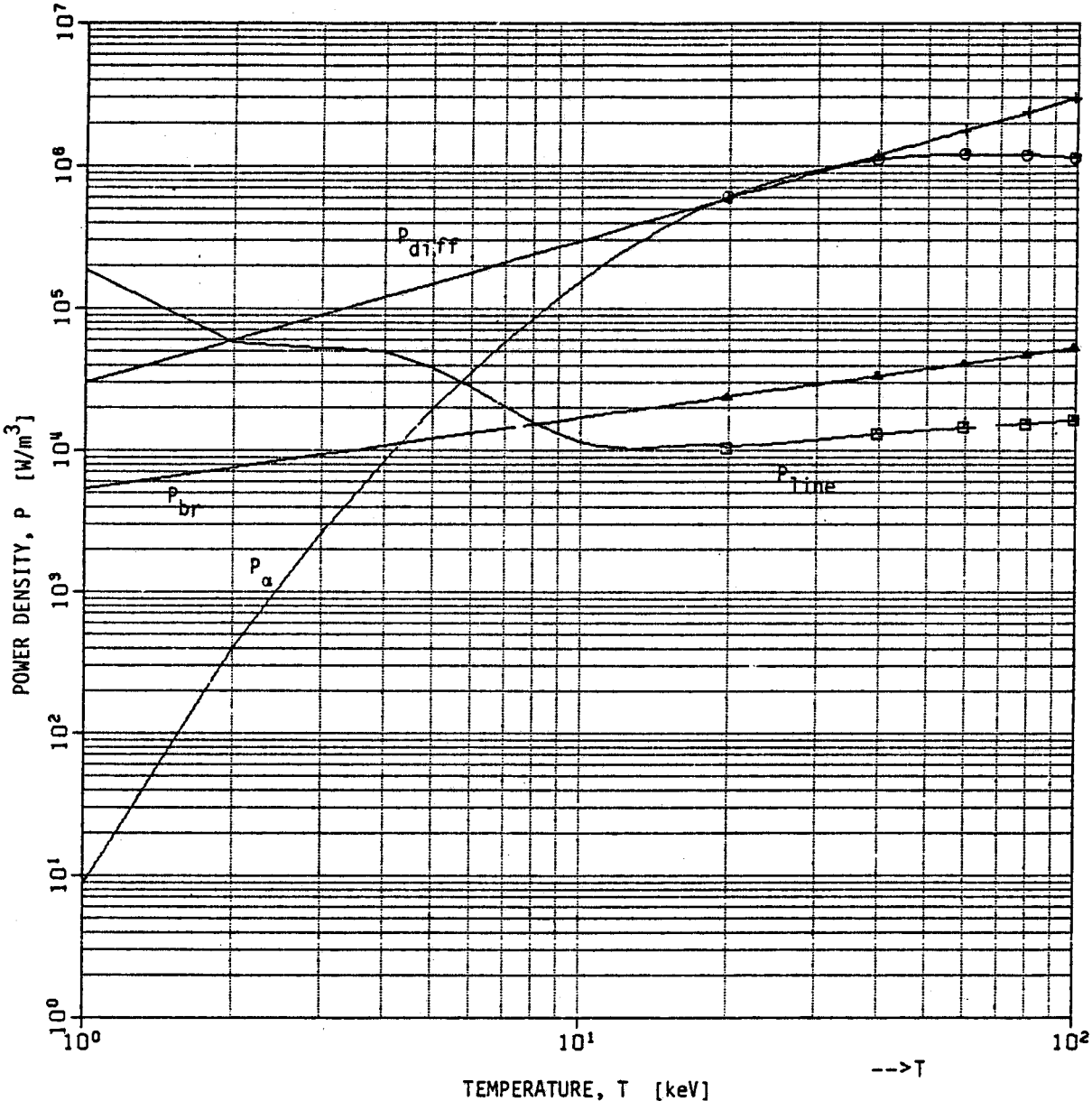
POWER DENSITY, P [W/m^3]
10^7
10^6
10^5
10^4
10^3
10^2
10^1
10^0
P_{diff}
P_{br}
P_{line}
P_α
10^0
10^1
10^2
-->T
TEMPERATURE, T [keV]

Fig. 3

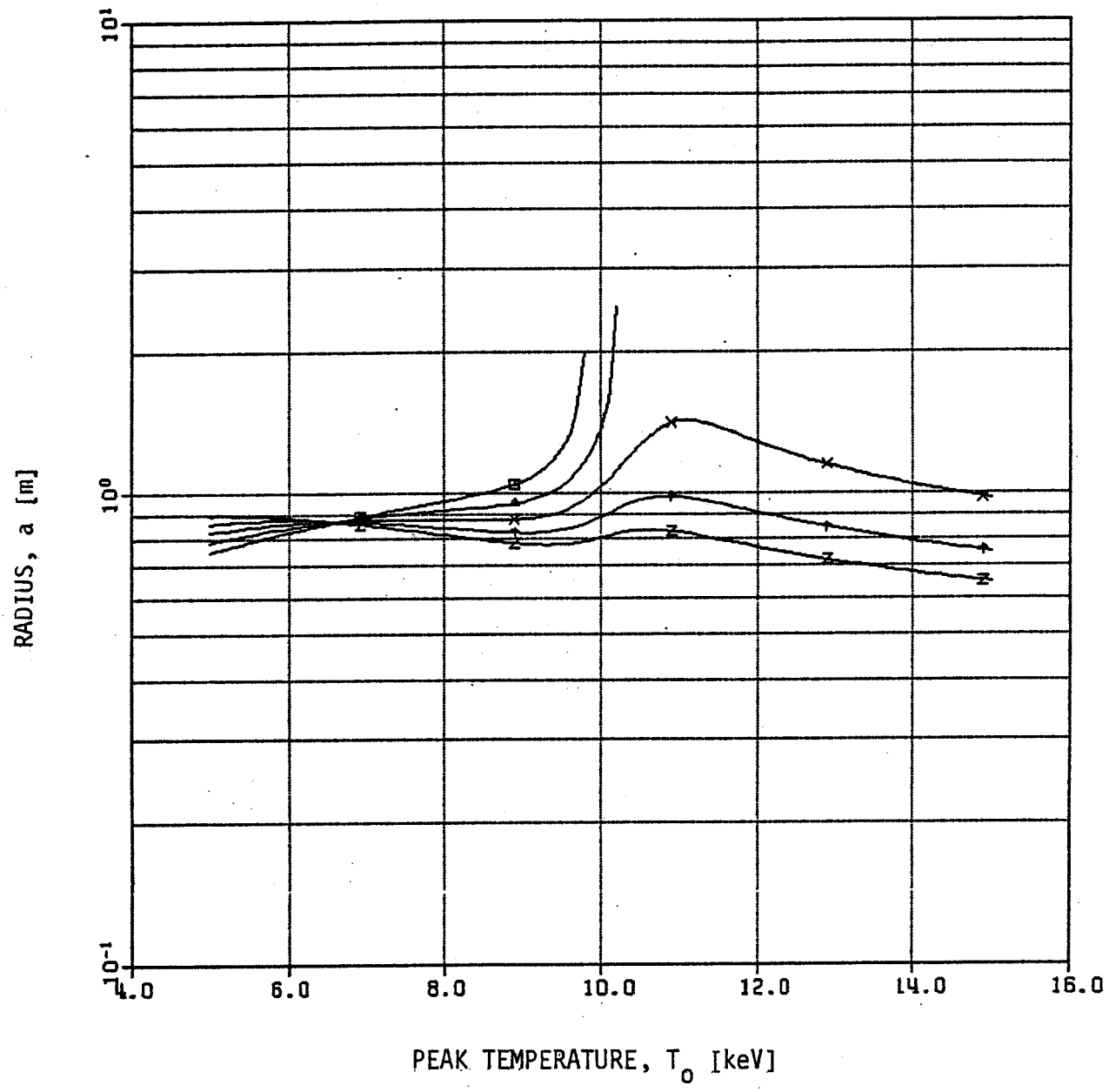
RADIUS, a [m]
10^1
10^0
10^{-1}
4.0
6.0
8.0
10.0
12.0
14.0
16.0
PEAK TEMPERATURE, T_o [keV]

Fig. 4a

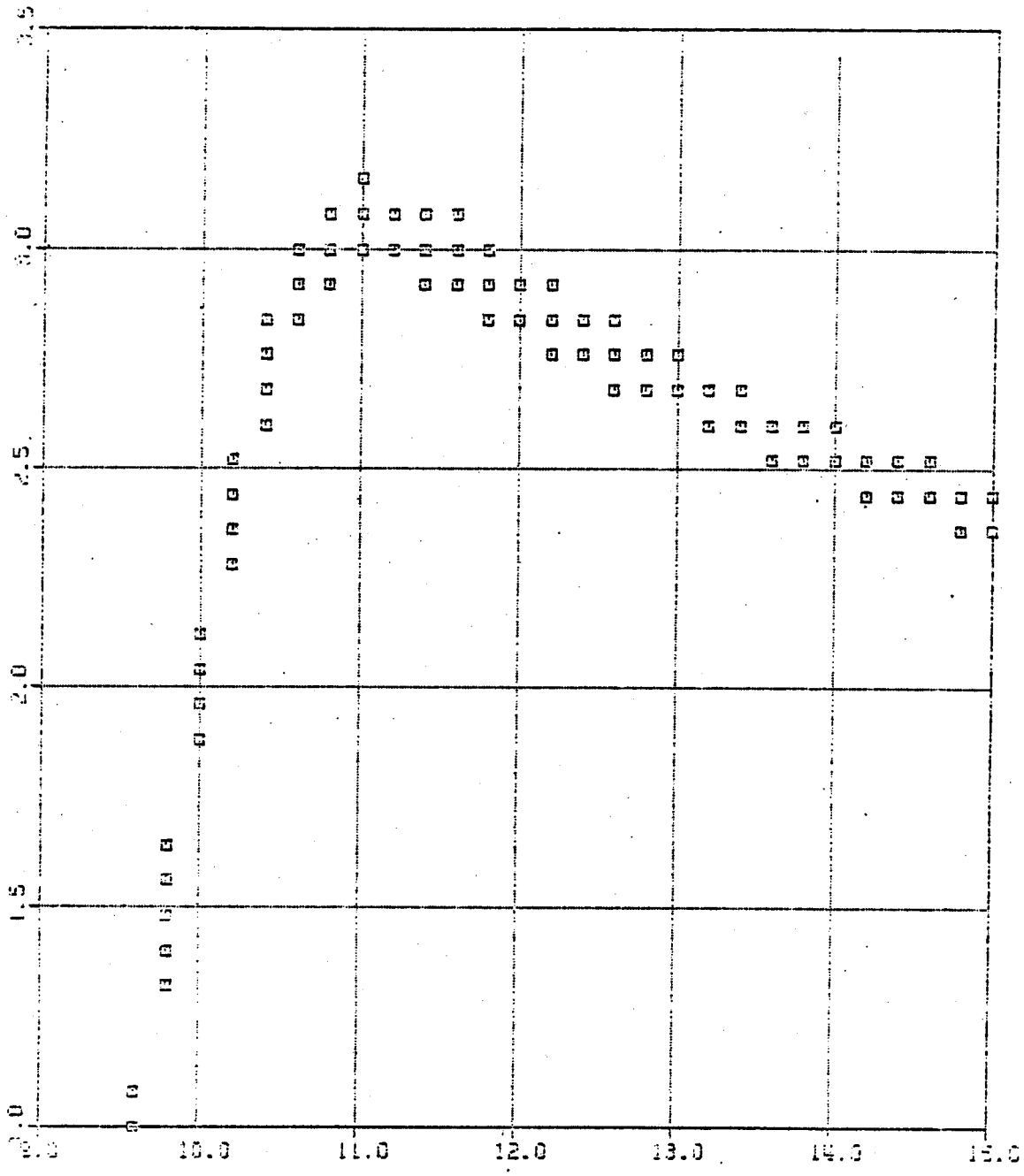
3.5
3.0
2.5
2.0
1.5
1.0
10.0
11.0
12.0
13.0
14.0
15.0
PEAK DENSITY, n_o [$10^{20}m^{-3}$]
PEAK TEMPERATURE, T_o [keV]

Fig. 4b

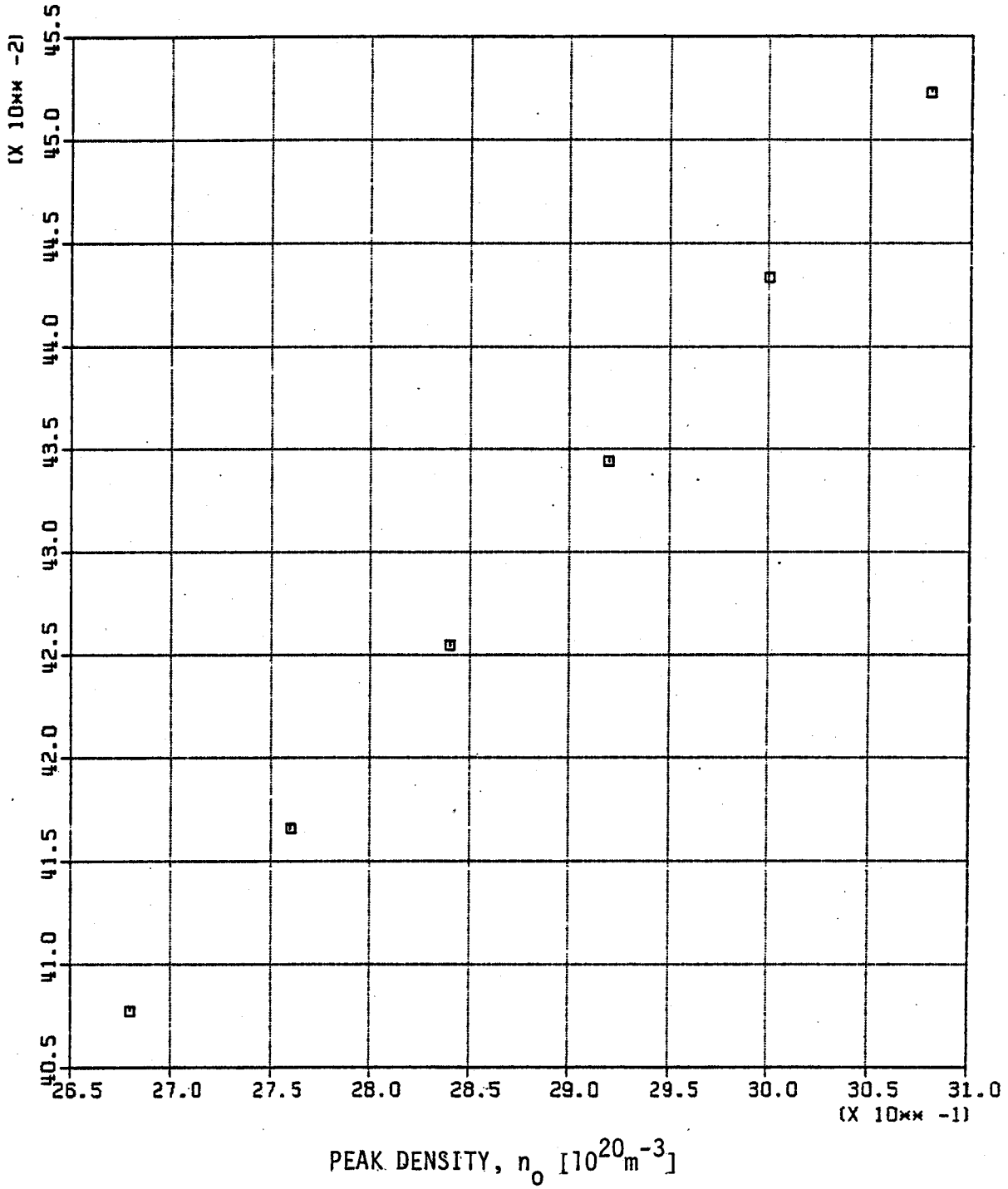
TOTAL REACTOR POWER OUTPUT, P_{out} [GW]
(X 10** -2)
45.5
45.0
44.5
44.0
43.5
43.0
42.5
42.0
41.5
41.0
40.5
26.5
27.0
27.5
28.0
28.5
29.0
29.5
30.0
30.5
31.0
(X 10** -1)
PEAK DENSITY, n_o [$10^{20}m^{-3}$]

Fig. 4c

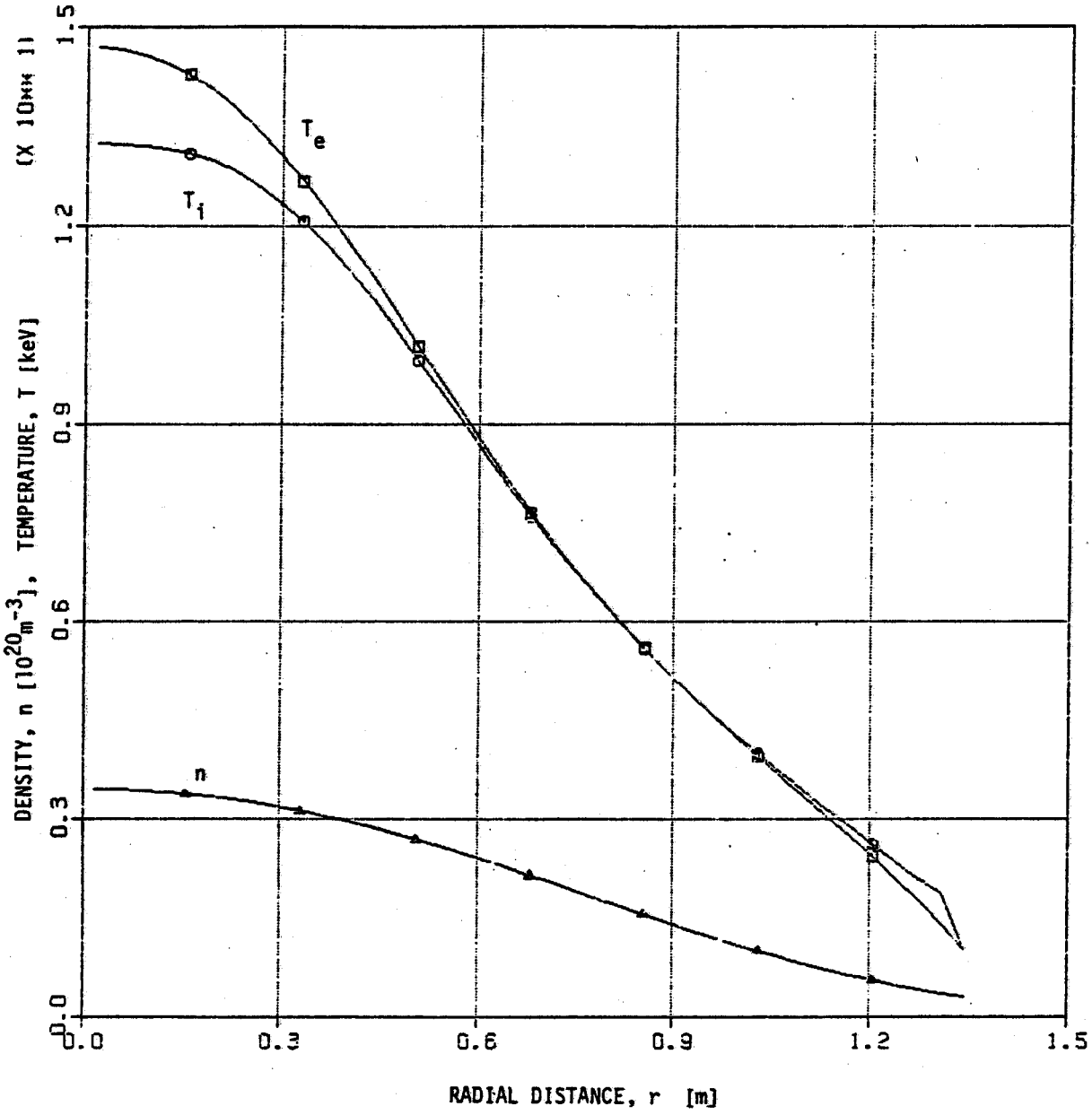
(X 10** 1)
1.5
1.2
0.9
0.6
0.3
0.0
T_e
T_i
n
DENSITY, n [$10^{20}m^{-3}$], TEMPERATURE, T [keV]
0.0
0.3
0.6
0.9
1.2
1.5
RADIAL DISTANCE, r [m]

Fig. 5a

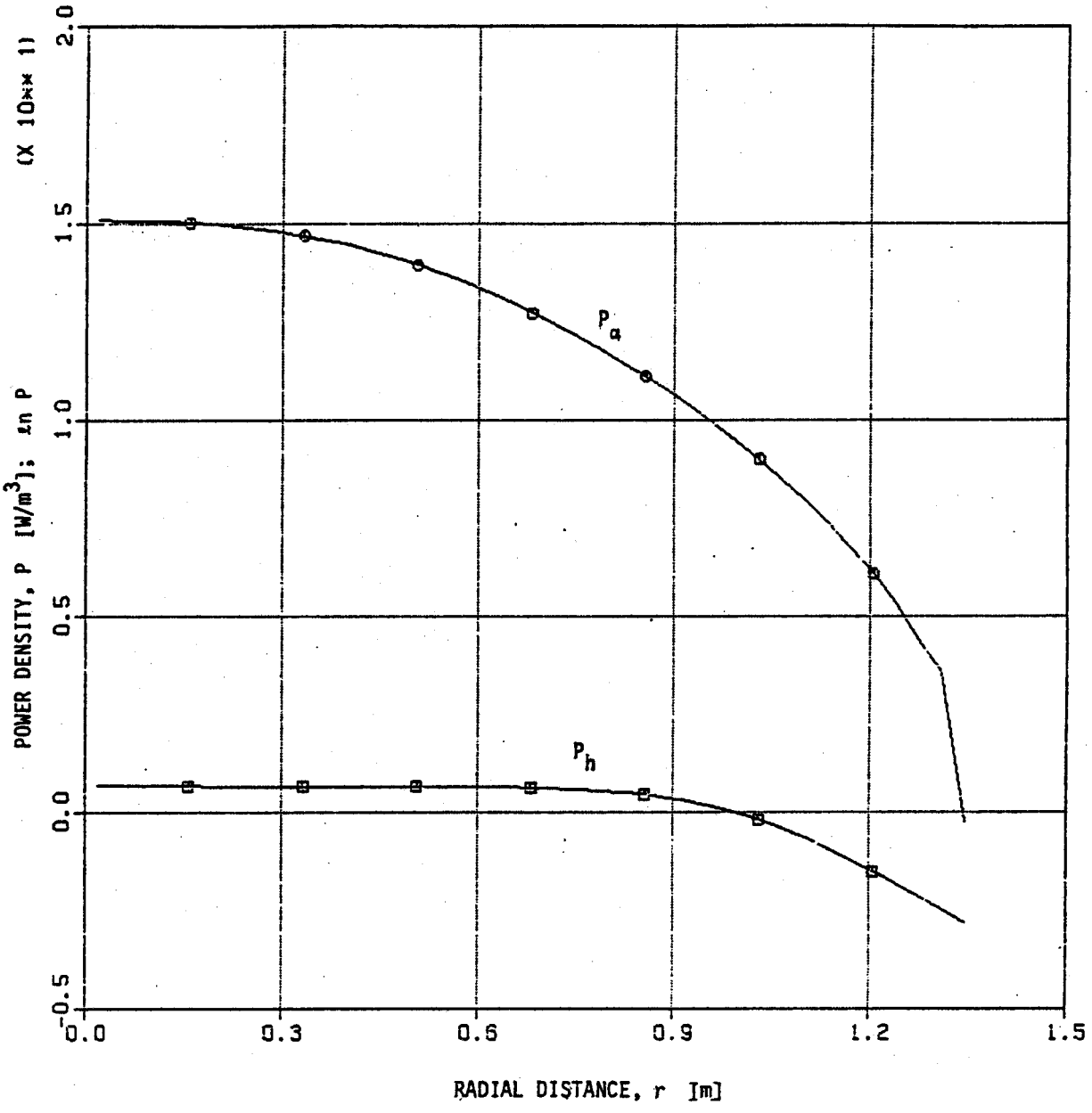
(X 10** 1)
2.0
1.5
1.0
0.5
0.0
-0.5
POWER DENSITY, P [W/m3]; ln P
P_α
P_h
0.0
0.3
0.6
0.9
1.2
1.5
RADIAL DISTANCE, r [m]

Fig. 5b

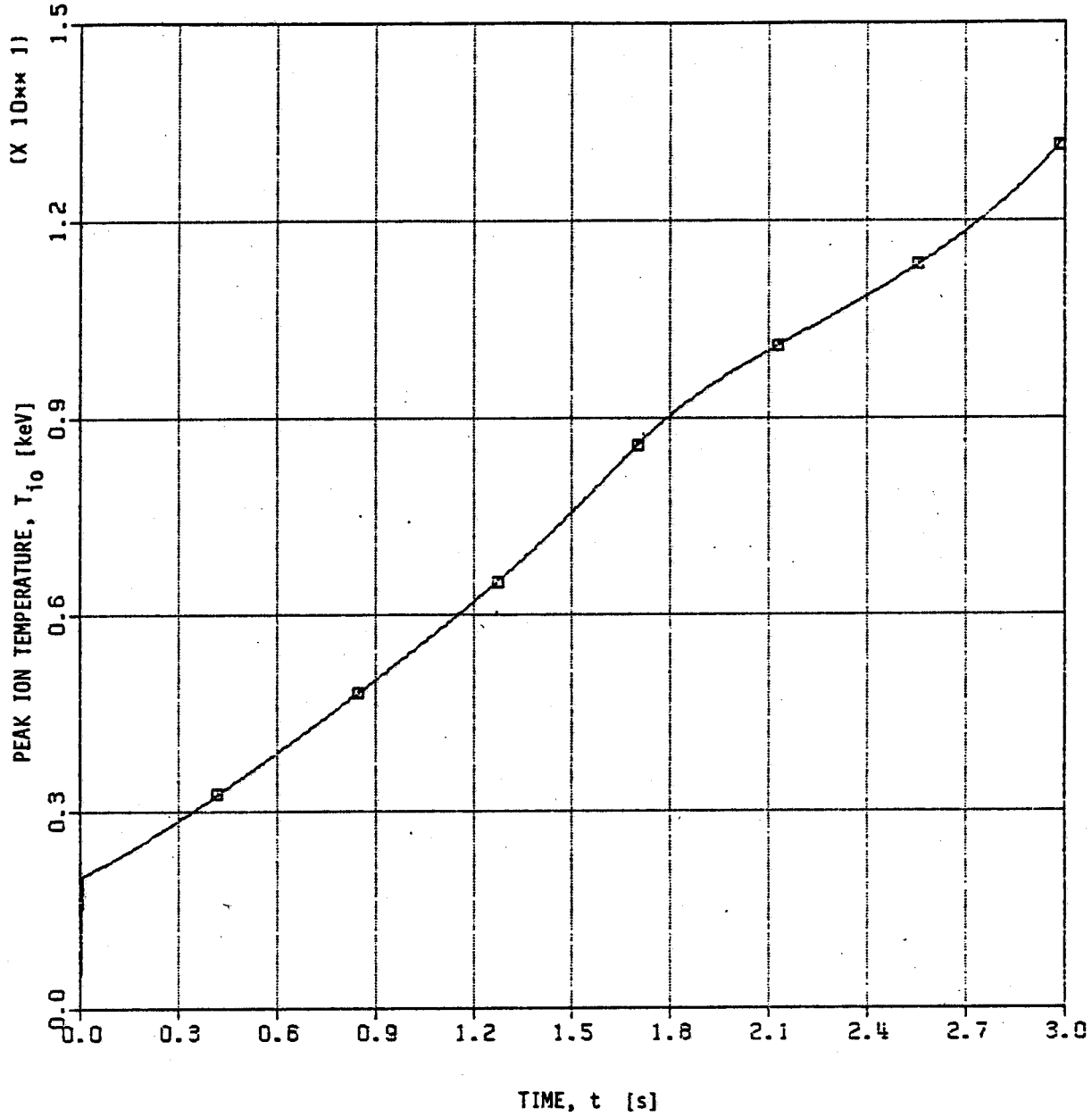
(X 10** 1)
1.5
1.2
0.9
0.6
0.3
0.0
PEAK ION TEMPERATURE, T_{io} [keV]
0.0
0.3
0.6
0.9
1.2
1.5
1.8
2.1
2.4
2.7
3.0
TIME, t [s]

Fig. 5c

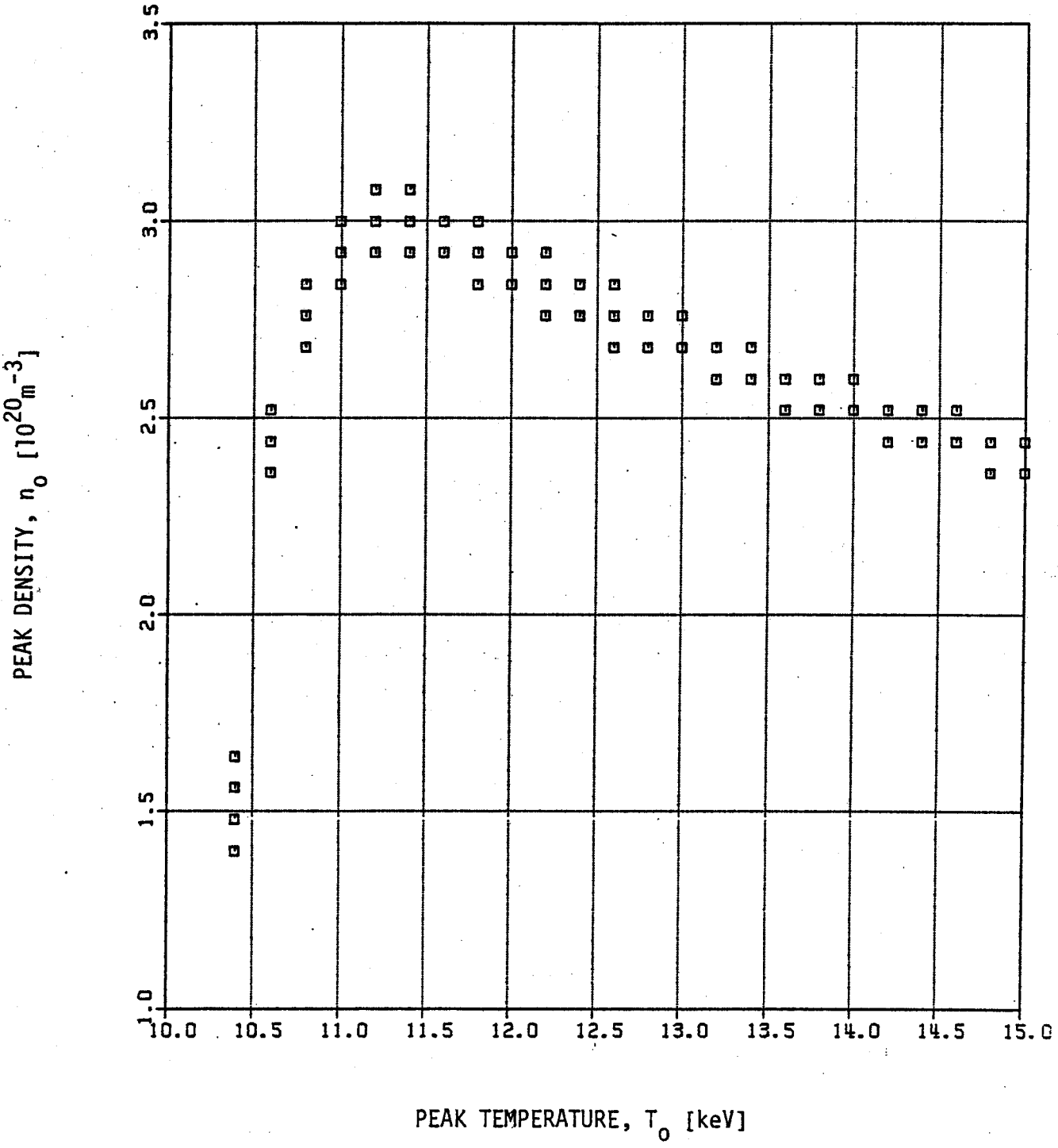
PEAK DENSITY, n_o [$10^{20} m^{-3}$]
3.5
3.0
2.5
2.0
1.5
1.0
10.0
10.5
11.0
11.5
12.0
12.5
13.0
13.5
14.0
14.5
15.0
PEAK TEMPERATURE, T_o [keV]

Fig. 6a

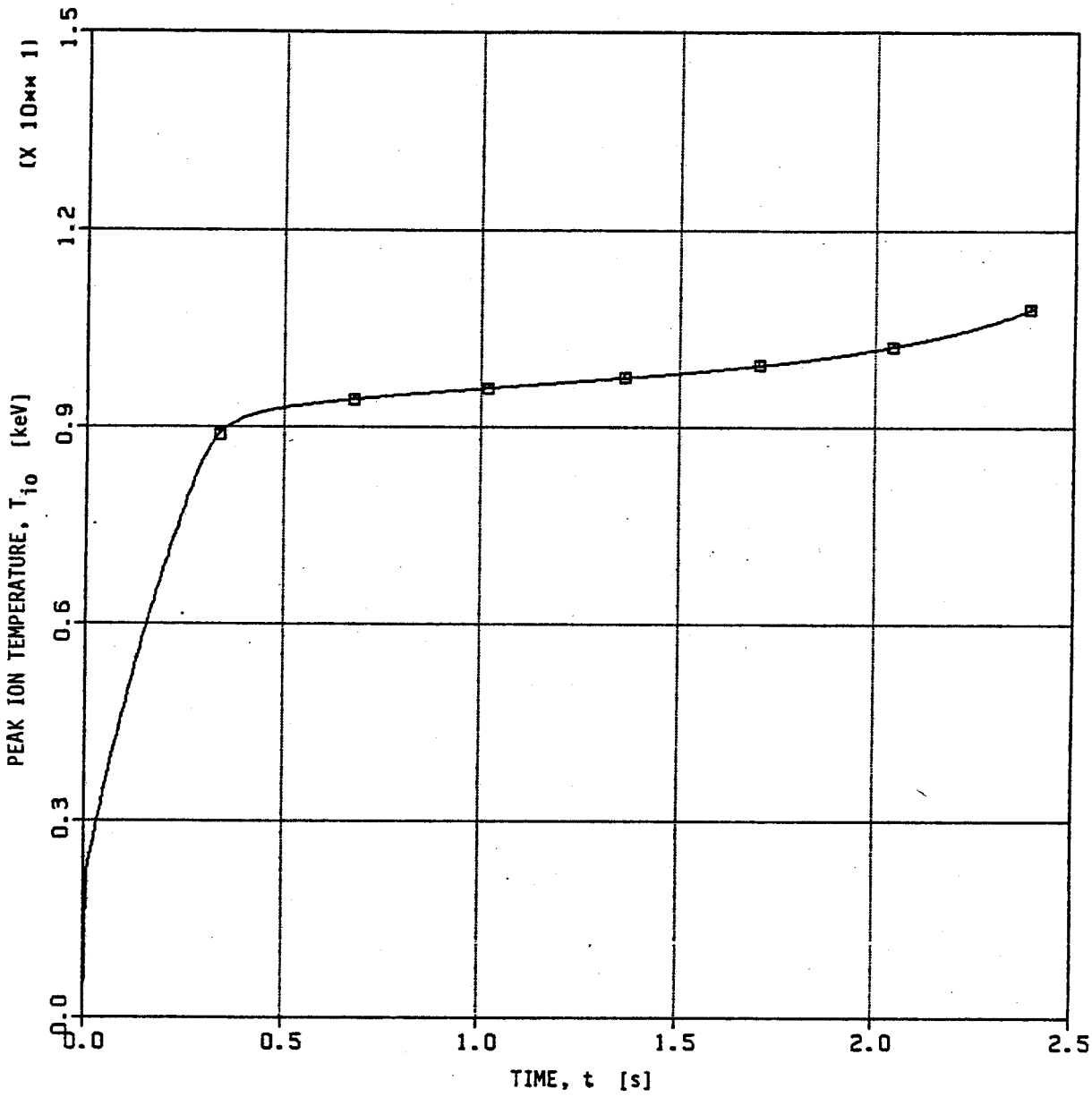
PEAK ION TEMPERATURE, T_{io} [keV]
(X 10** 1)
1.5
1.2
0.9
0.6
0.3
0.0
0.0
0.5
1.0
1.5
2.0
2.5
TIME, t [s]

Fig. 6b

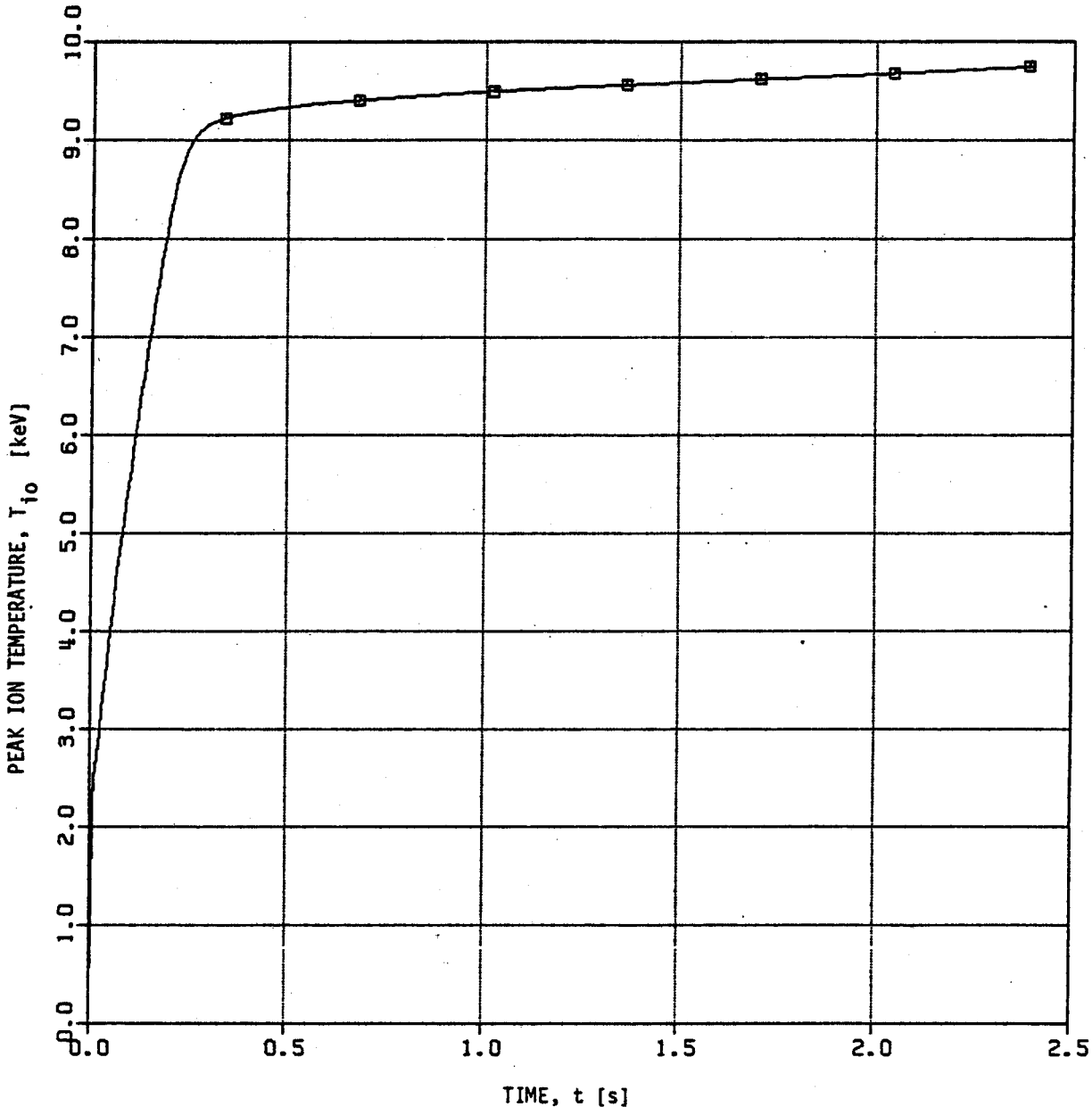
PEAK ION TEMPERATURE, T_{io} [keV]
0.0
1.0
2.0
3.0
4.0
5.0
6.0
7.0
8.0
9.0
10.0
0.0
0.5
1.0
1.5
2.0
2.5
TIME, t [s]

Fig. 6c

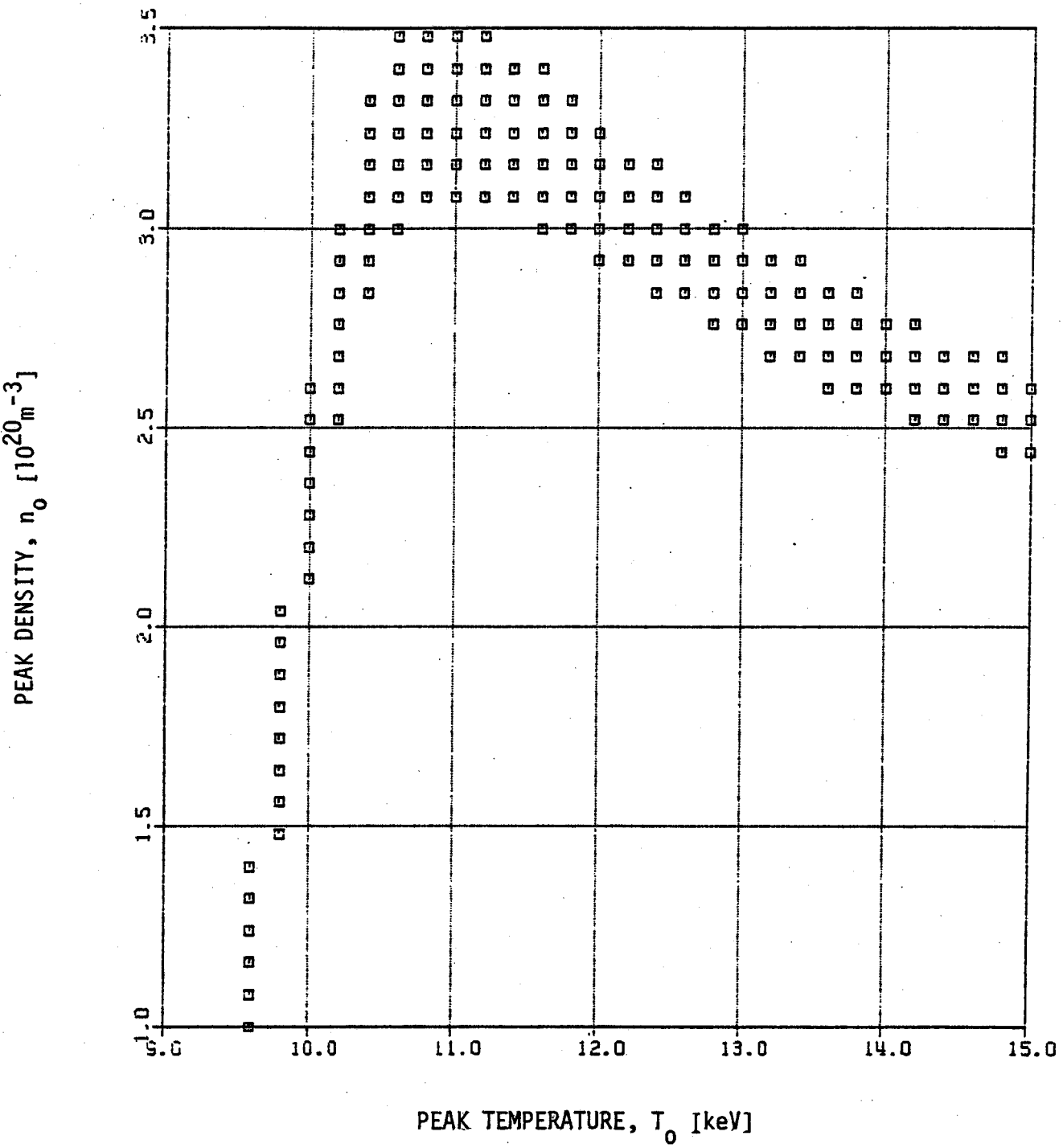
PEAK DENSITY, n_o [$10^{20} m^{-3}$]
3.5
3.0
2.5
2.0
1.5
1.0
9.0
10.0
11.0
12.0
13.0
14.0
15.0
PEAK TEMPERATURE, T_o [keV]

Fig. 7a

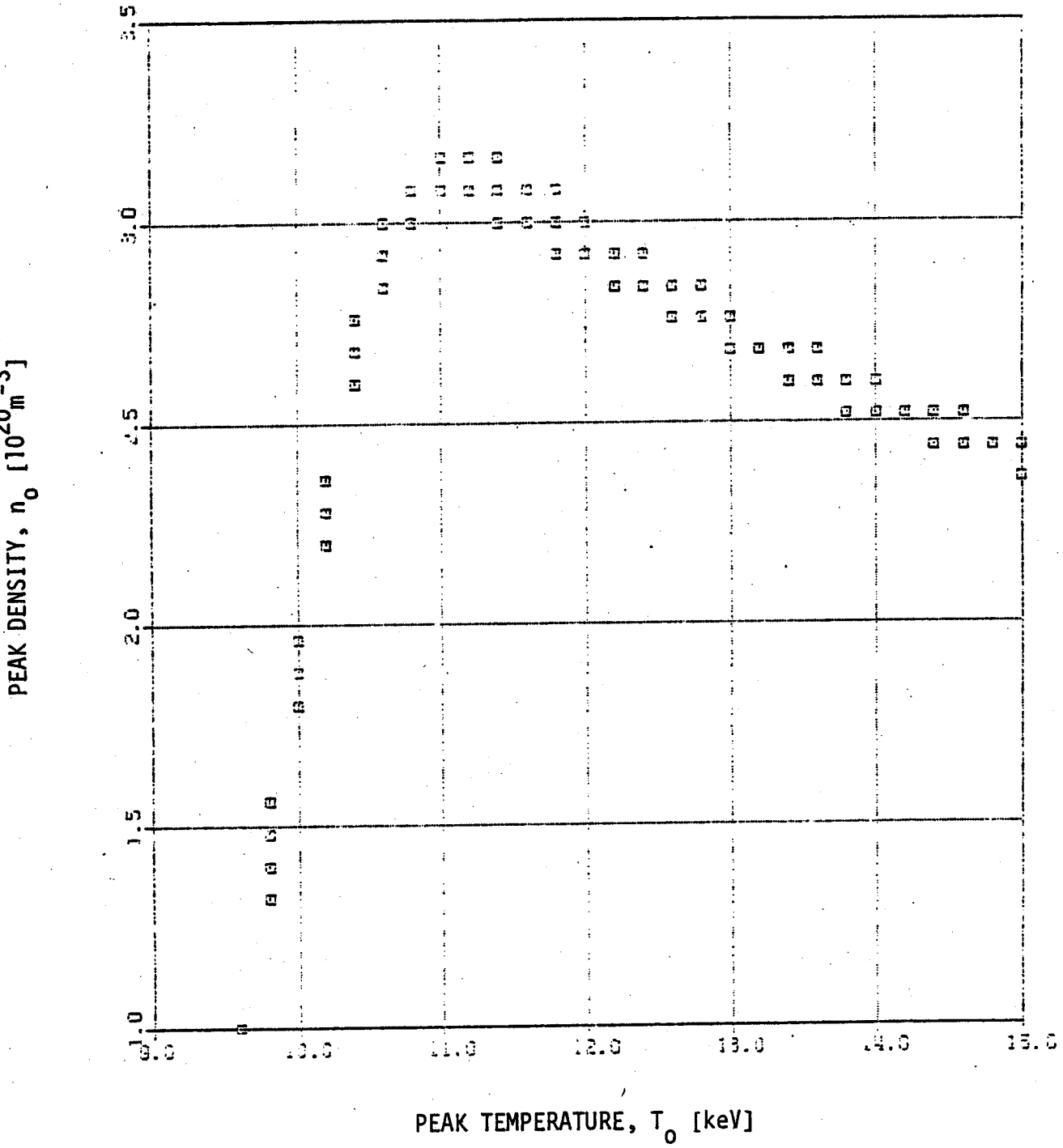
PEAK DENSITY, n_o [$10^{20}m^{-3}$]
3.5
3.0
2.5
2.0
1.5
1.0
9.0
10.0
11.0
12.0
13.0
14.0
15.0
PEAK TEMPERATURE, T_o [keV]

Fig. 7b

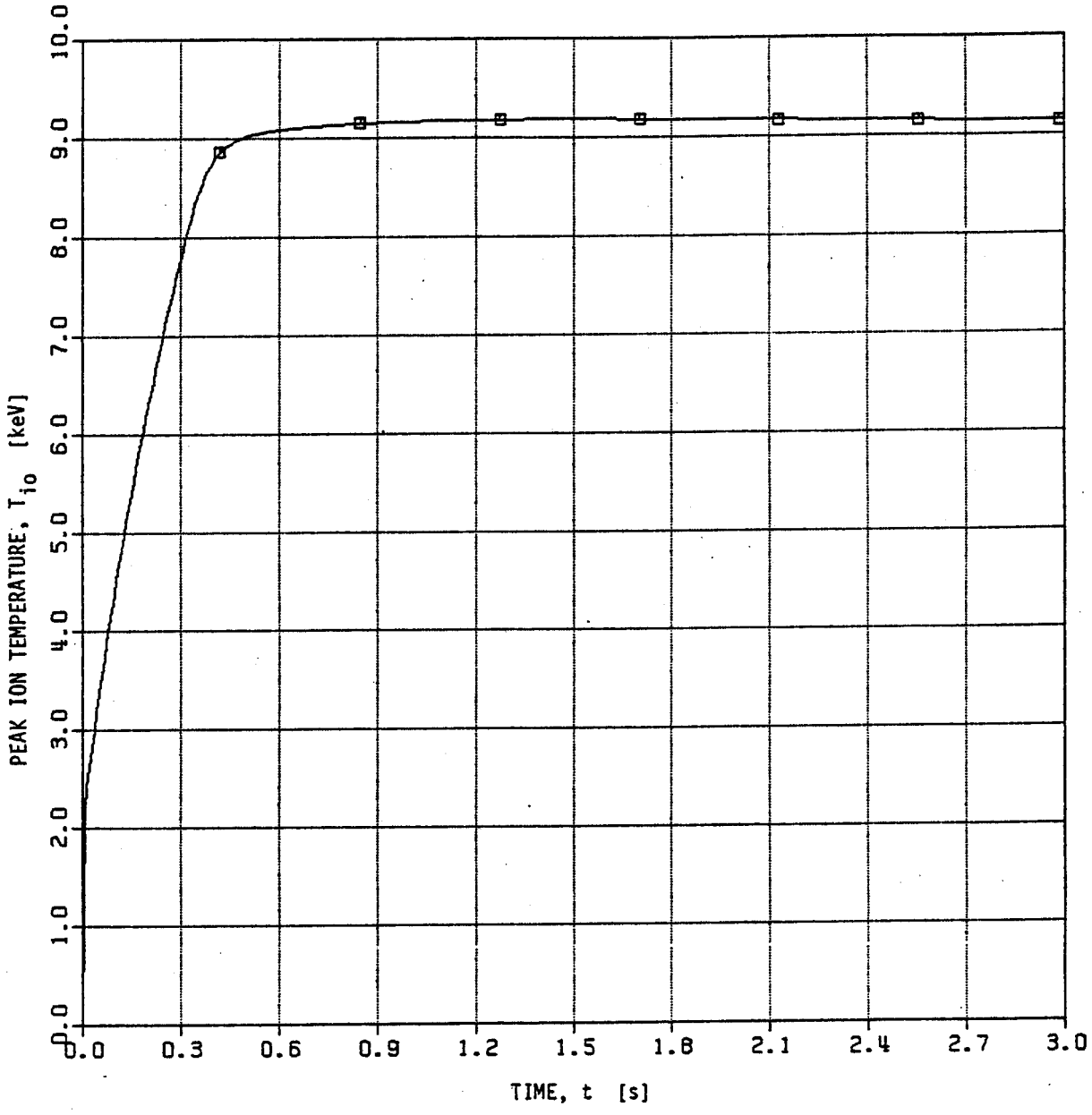
PEAK ION TEMPERATURE, T_{io} [keV]
0.0
1.0
2.0
3.0
4.0
5.0
6.0
7.0
8.0
9.0
10.0
0.0
0.3
0.6
0.9
1.2
1.5
1.8
2.1
2.4
2.7
3.0
TIME, t [s]

Fig. 8a

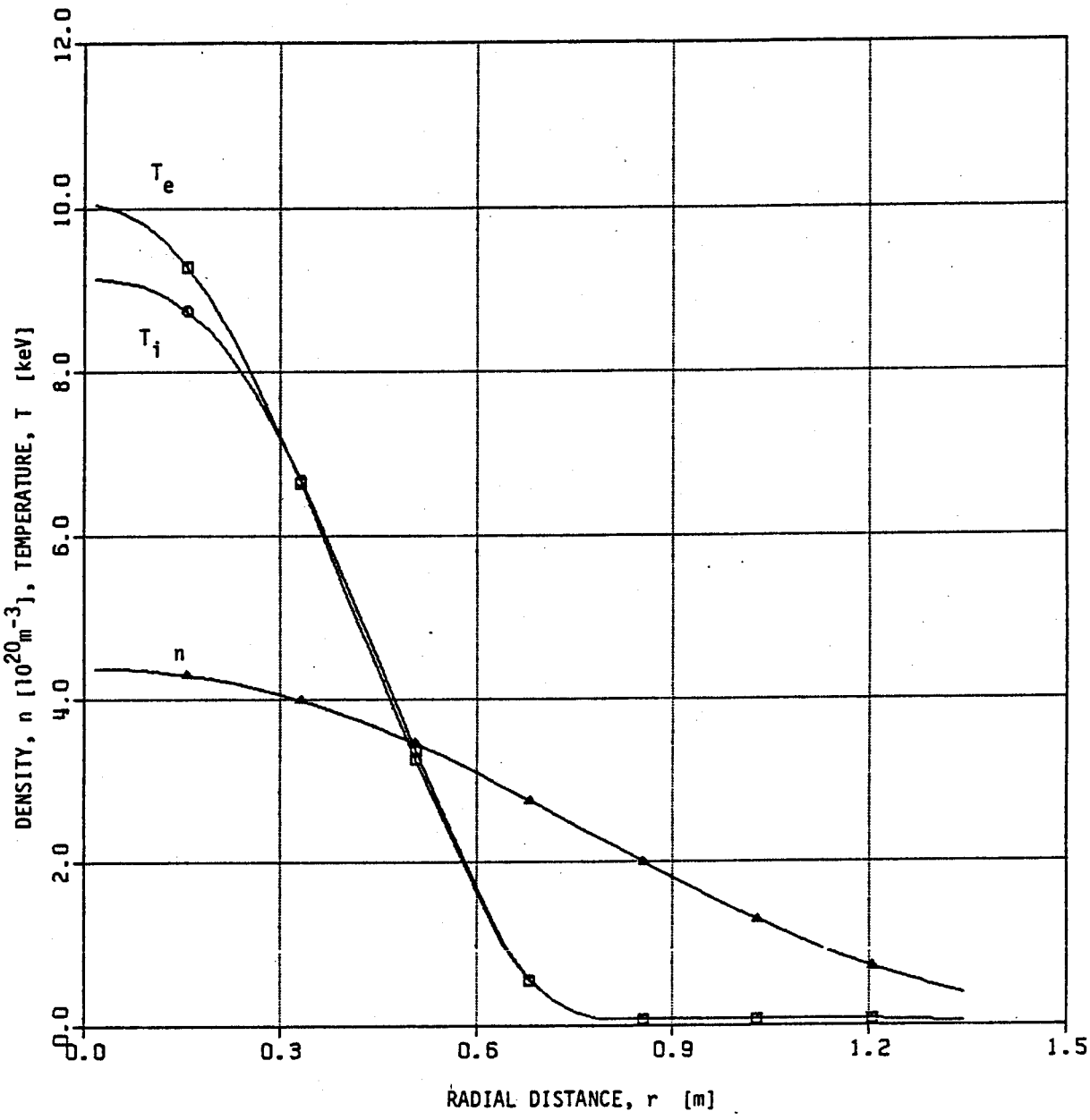
12.0
10.0
8.0
6.0
4.0
2.0
0.0
T_e
T_i
n
DENSITY, n [$10^{20}m^{-3}$], TEMPERATURE, T [keV]
0.0
0.3
0.6
0.9
1.2
1.5
RADIAL DISTANCE, r [m]

Fig. 8b

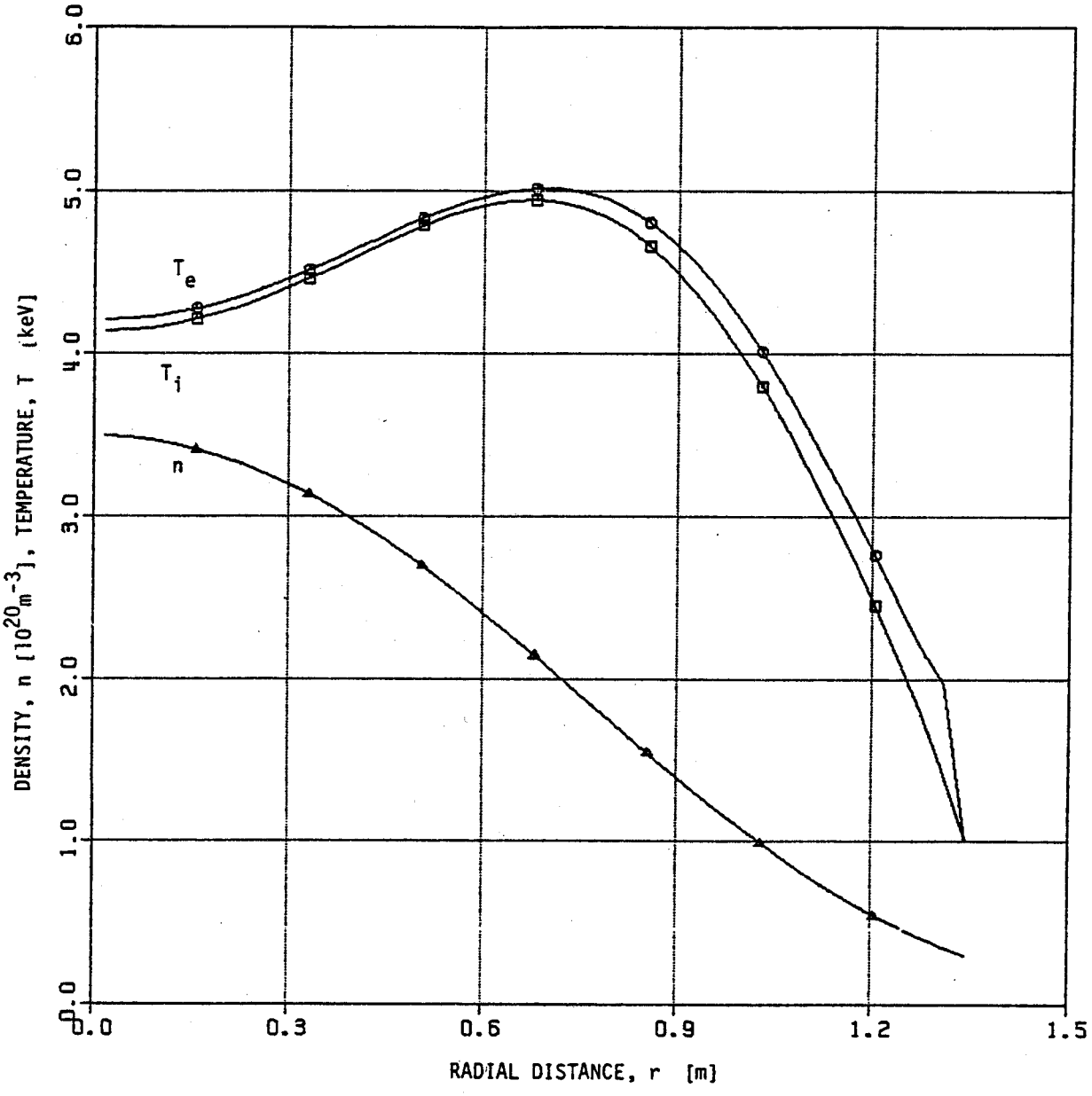
DENSITY, n [$10^{20}m^{-3}$], TEMPERATURE, T [keV]
RADIAL DISTANCE, r [m]
T_e
T_i
n
0.0
1.0
2.0
3.0
4.0
5.0
6.0
0.0
0.3
0.6
0.9
1.2
1.5

Fig. 8c

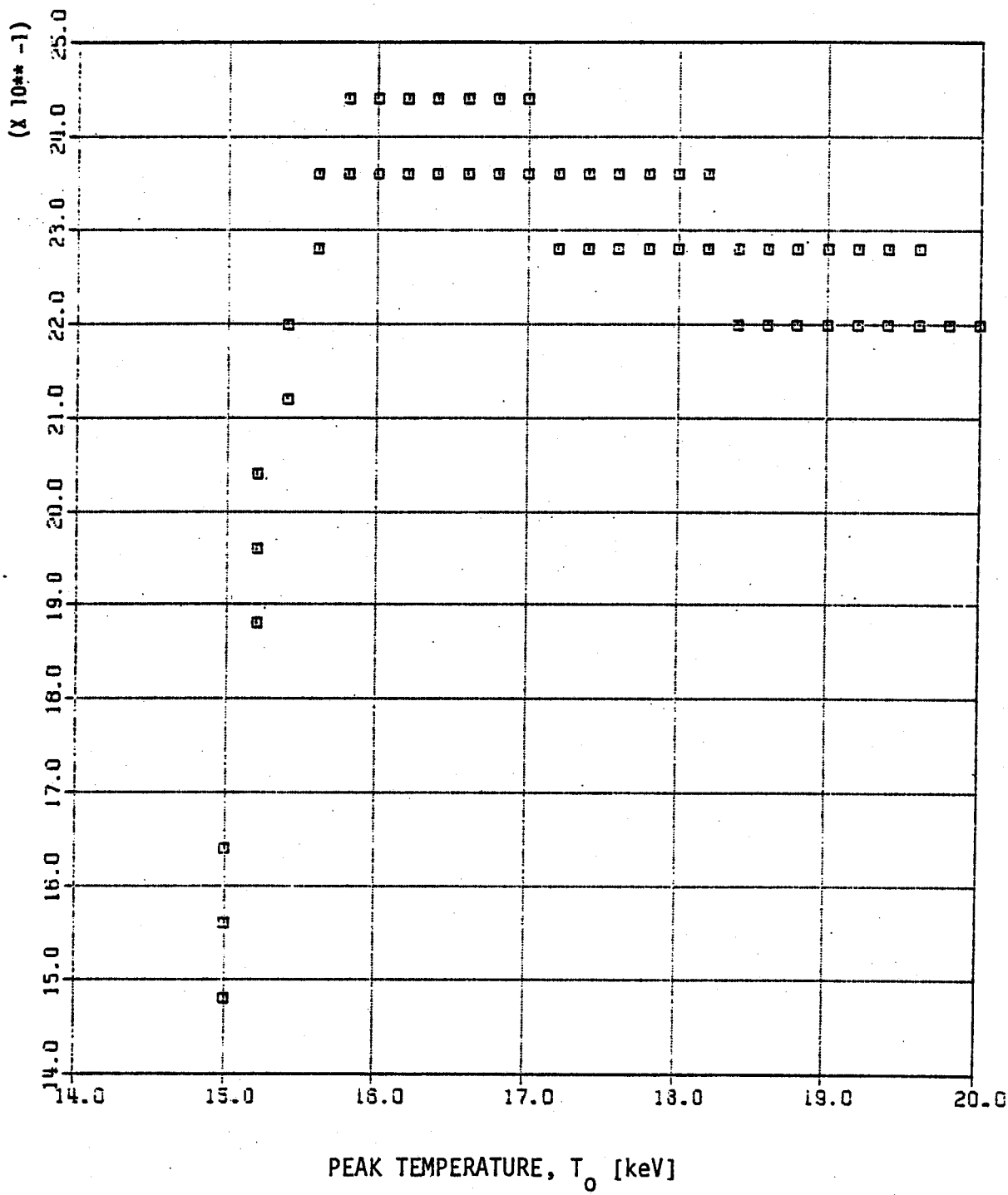
(X 10** -1)
25.0
24.0
23.0
22.0
21.0
20.0
19.0
18.0
17.0
16.0
15.0
14.0
14.0
15.0
16.0
17.0
18.0
19.0
20.0
PEAK DENSITY, n_o [$10^{20} m^{-3}$]
PEAK TEMPERATURE, T_o [keV]

Fig. 9a

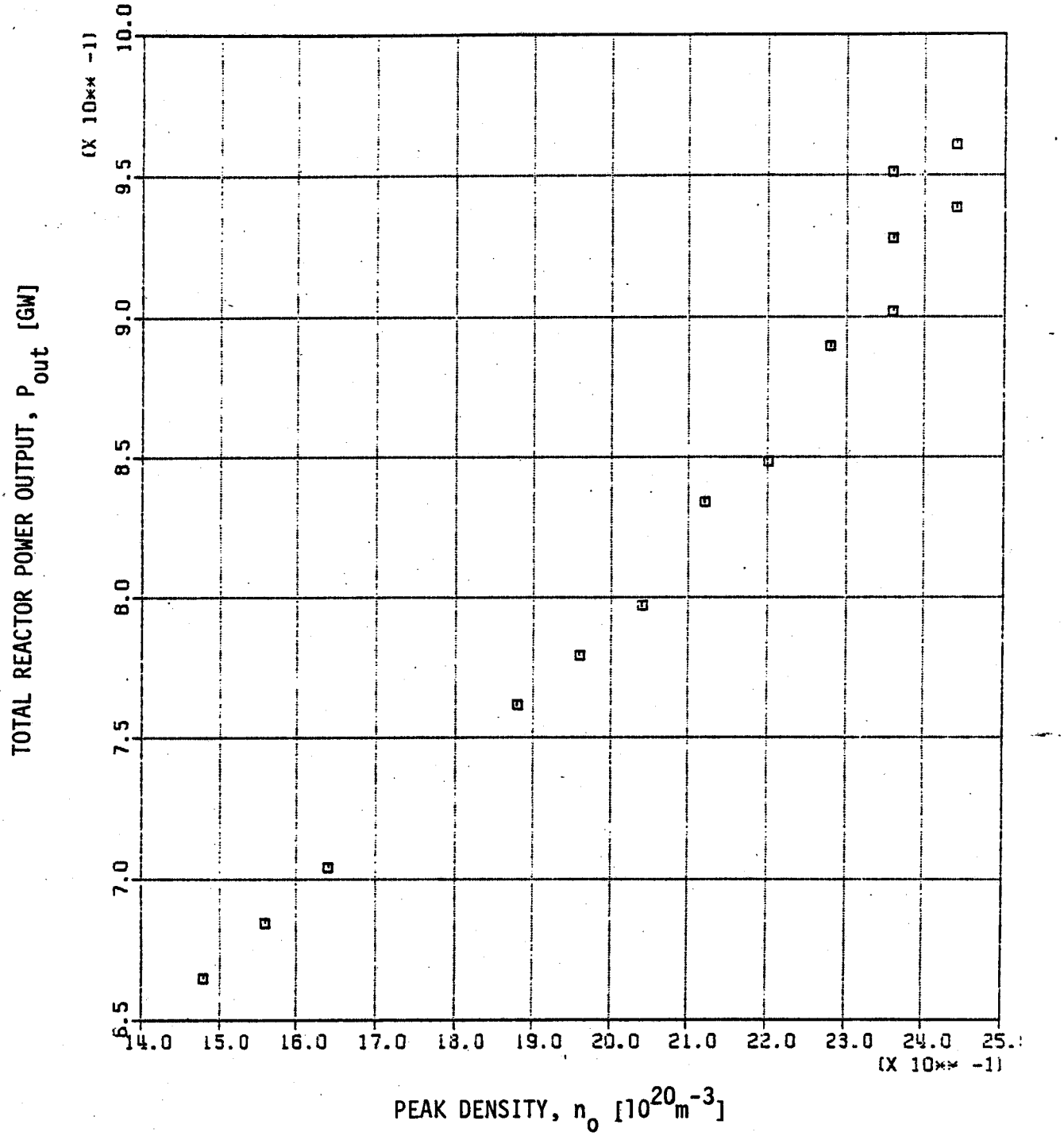
TOTAL REACTOR POWER OUTPUT, P_{out} [GW]
(X 10** -1)
10.0
9.5
9.0
8.5
8.0
7.5
7.0
6.5
14.0
15.0
16.0
17.0
18.0
19.0
20.0
21.0
22.0
23.0
24.0
25.
(X 10** -1)
PEAK DENSITY, n_o [$10^{20}m^{-3}$]

Fig. 9b

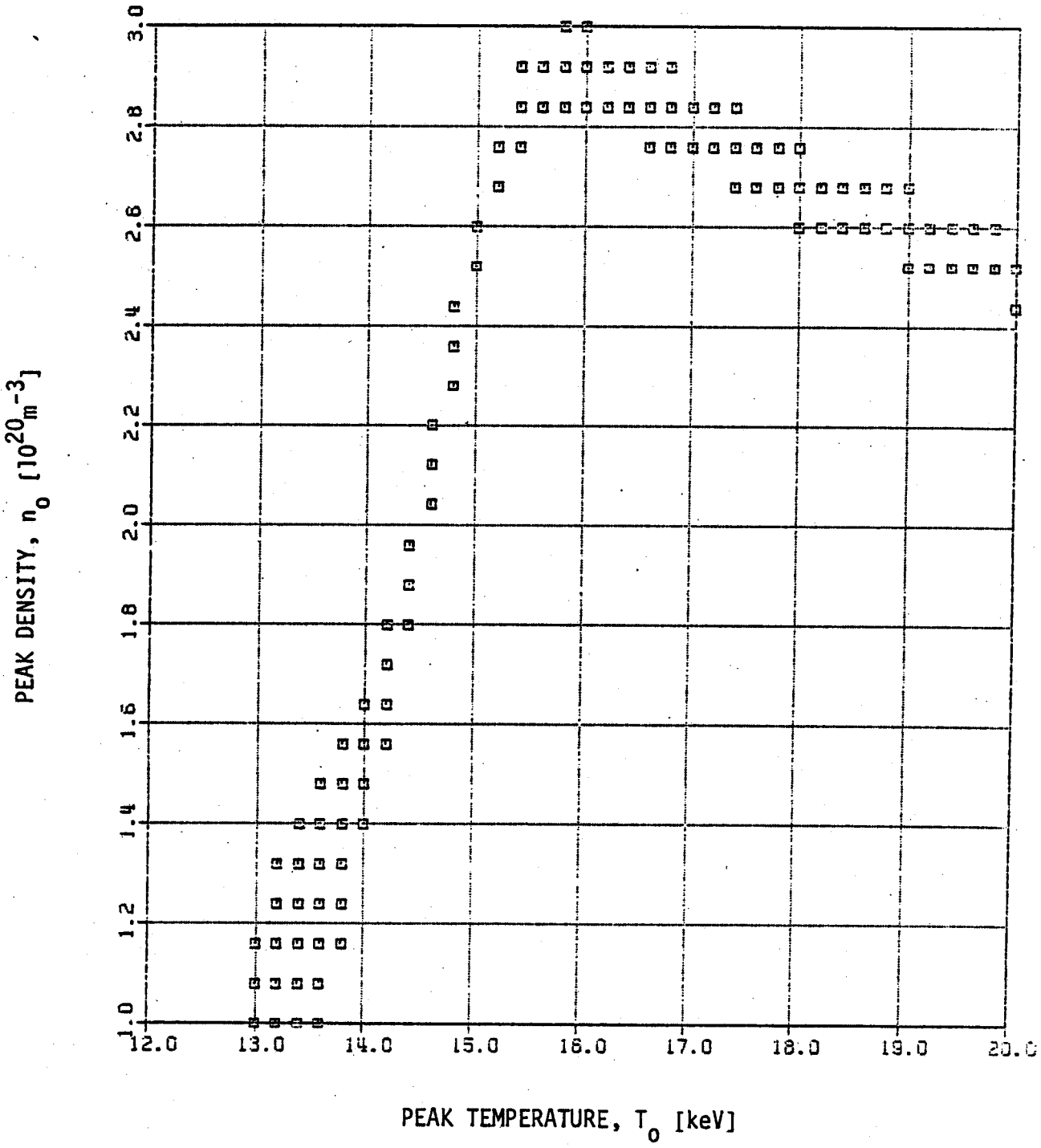
PEAK DENSITY, n_o [$10^{20} m^{-3}$]
3.0
2.8
2.6
2.4
2.2
2.0
1.8
1.6
1.4
1.2
1.0
12.0
13.0
14.0
15.0
16.0
17.0
18.0
19.0
20.0
PEAK TEMPERATURE, T_o [keV]

Fig. 10a

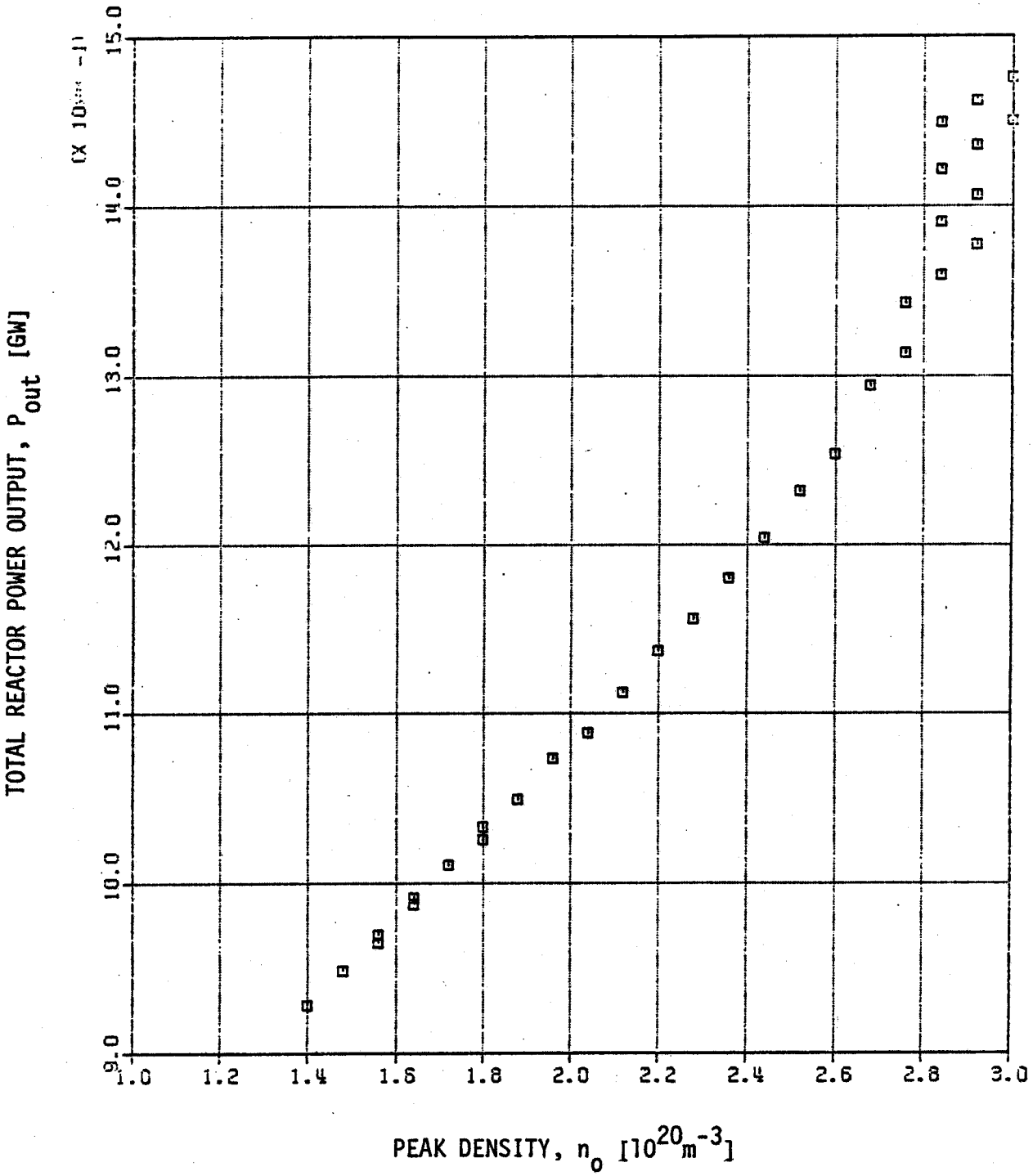
TOTAL REACTOR POWER OUTPUT, P_{out} [GW]
9.0
10.0
11.0
12.0
13.0
14.0
15.0
1.0
1.2
1.4
1.6
1.8
2.0
2.2
2.4
2.6
2.8
3.0
PEAK DENSITY, n_o [$10^{20}m^{-3}$]

Fig. 10b

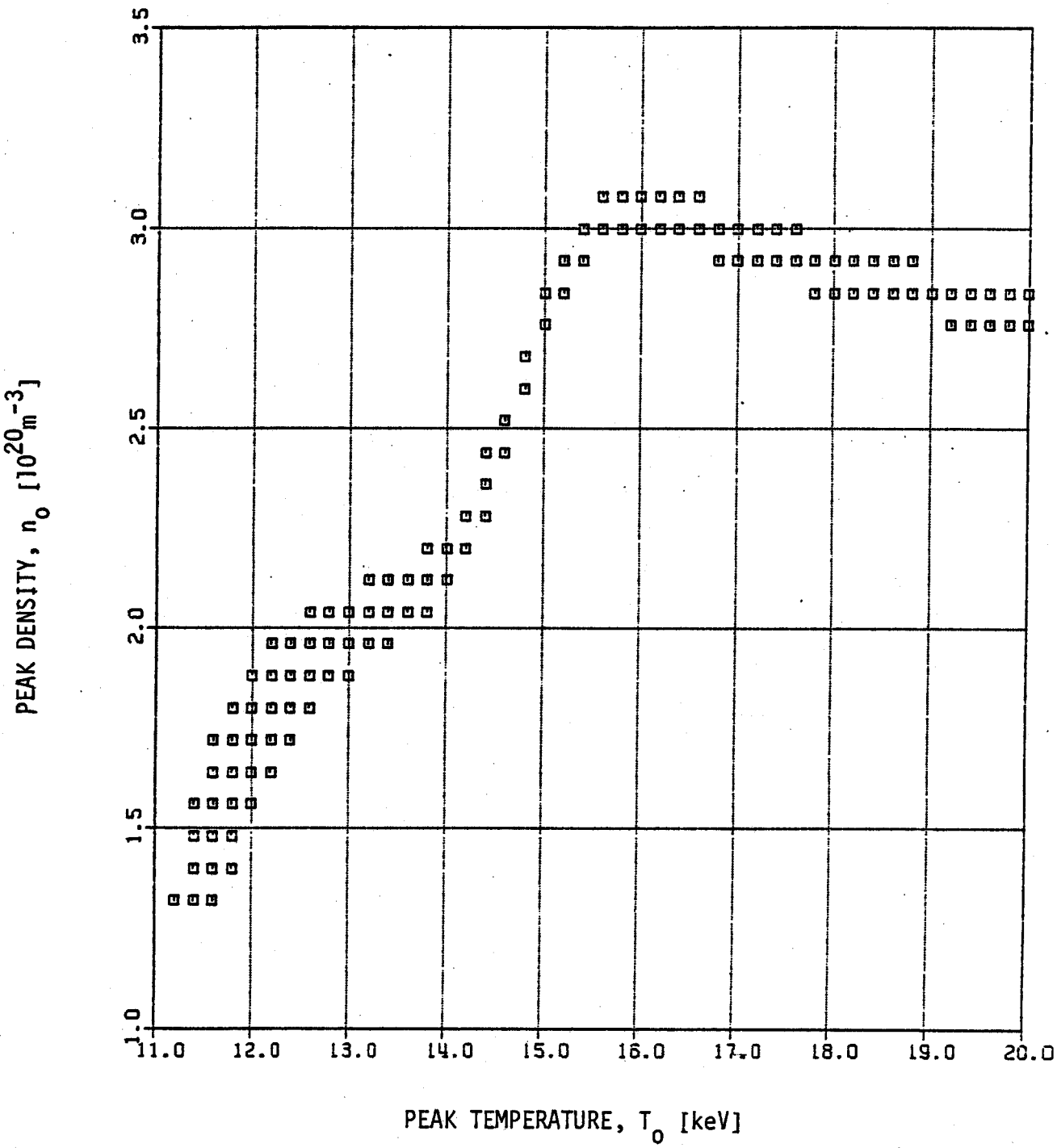
PEAK DENSITY, n_o [$10^{20} m^{-3}$]
3.5
3.0
2.5
2.0
1.5
1.0
11.0
12.0
13.0
14.0
15.0
16.0
17.0
18.0
19.0
20.0
PEAK TEMPERATURE, T_o [keV]

Fig. 11a

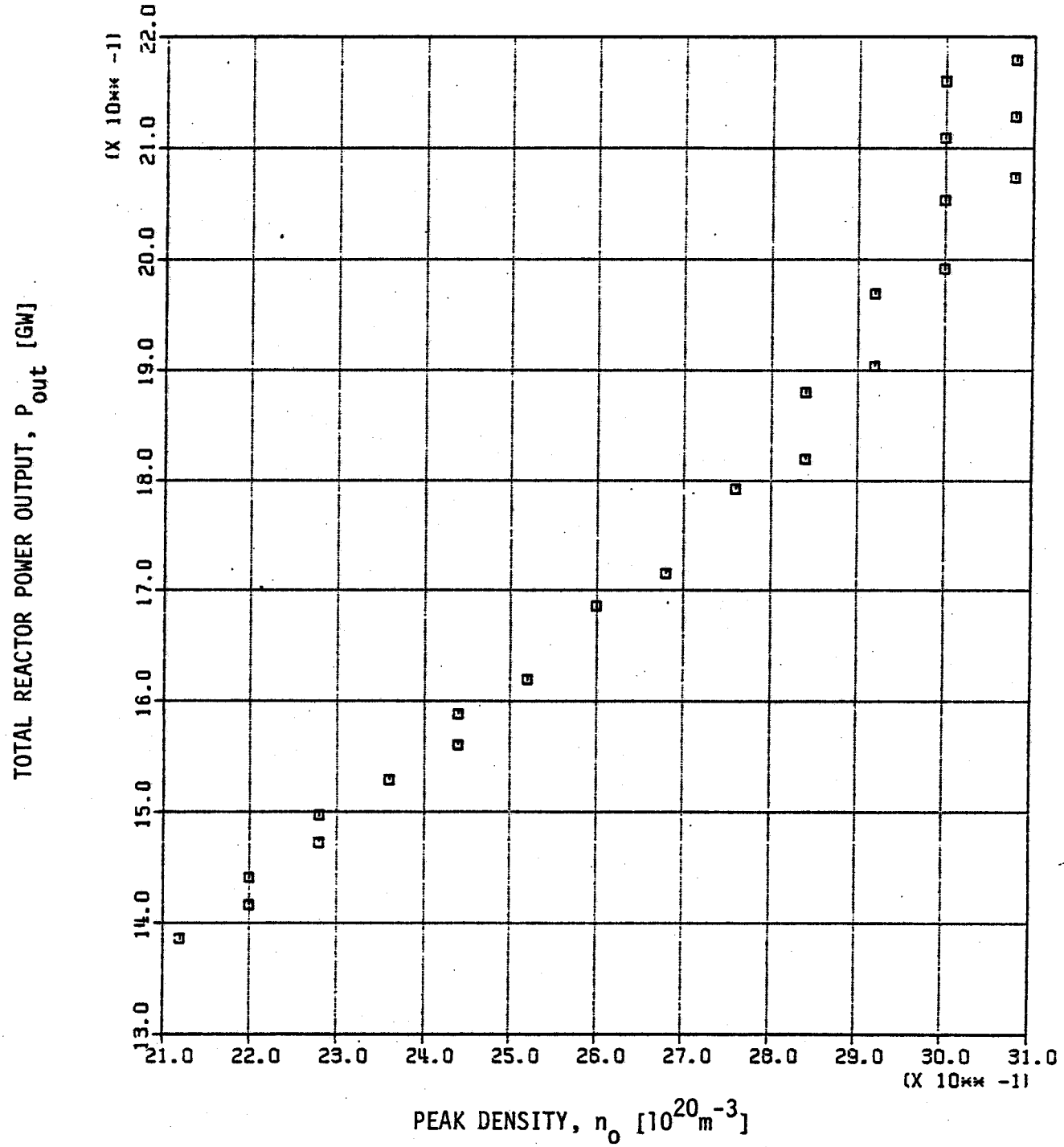
TOTAL REACTOR POWER OUTPUT, P_{out} [GW]
(X 10** -1)
22.0
21.0
20.0
19.0
18.0
17.0
16.0
15.0
14.0
13.0
21.0
22.0
23.0
24.0
25.0
26.0
27.0
28.0
29.0
30.0
31.0
(X 10** -1)
PEAK DENSITY, n_o [$10^{20}m^{-3}$]

Fig. 11b

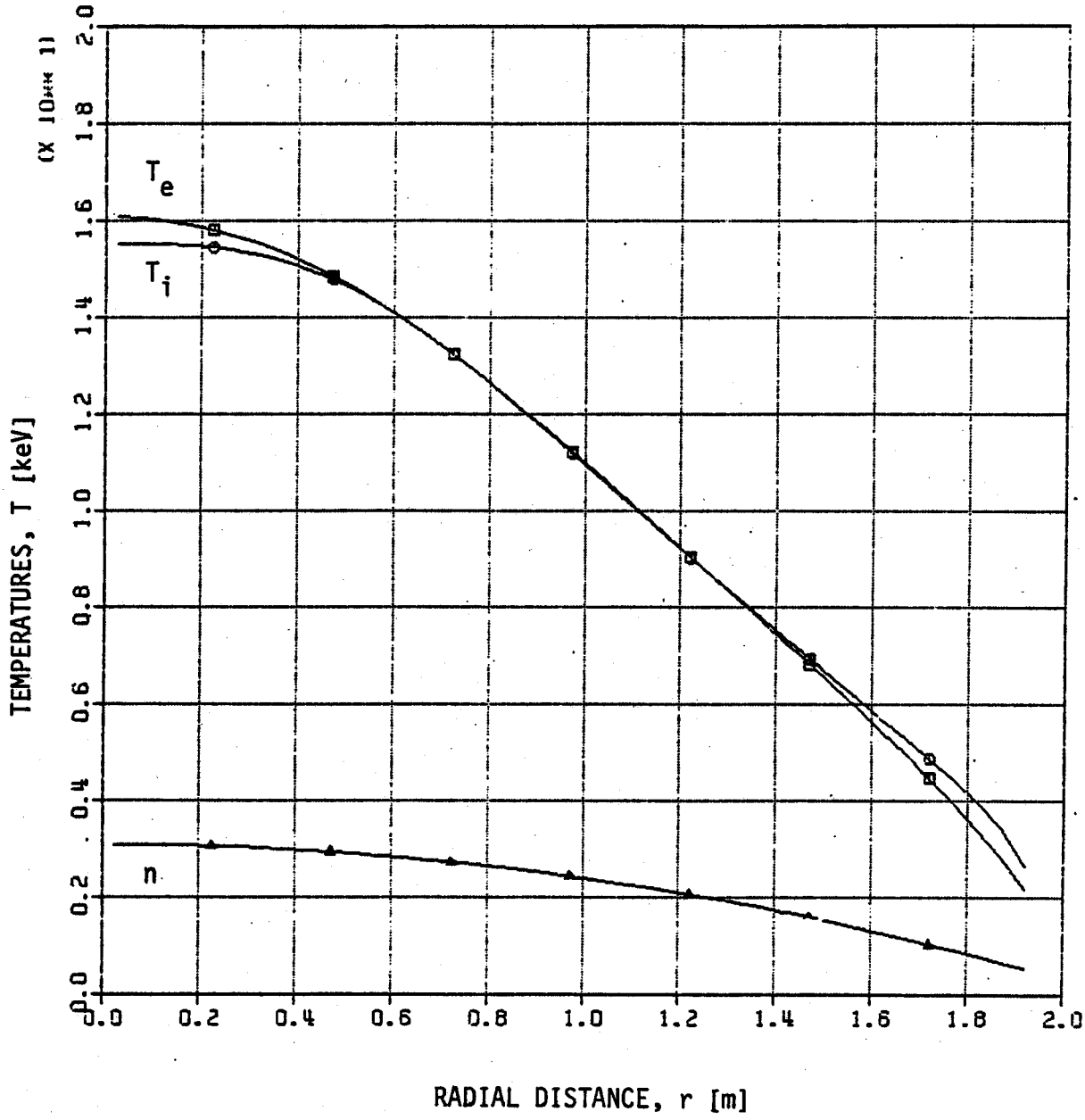
TEMPERATURES, T [keV]
(X 10**19 1)
T_e
T_i
n
0.0
0.2
0.4
0.6
0.8
1.0
1.2
1.4
1.6
1.8
2.0
RADIAL DISTANCE, r [m]

Fig. 12a

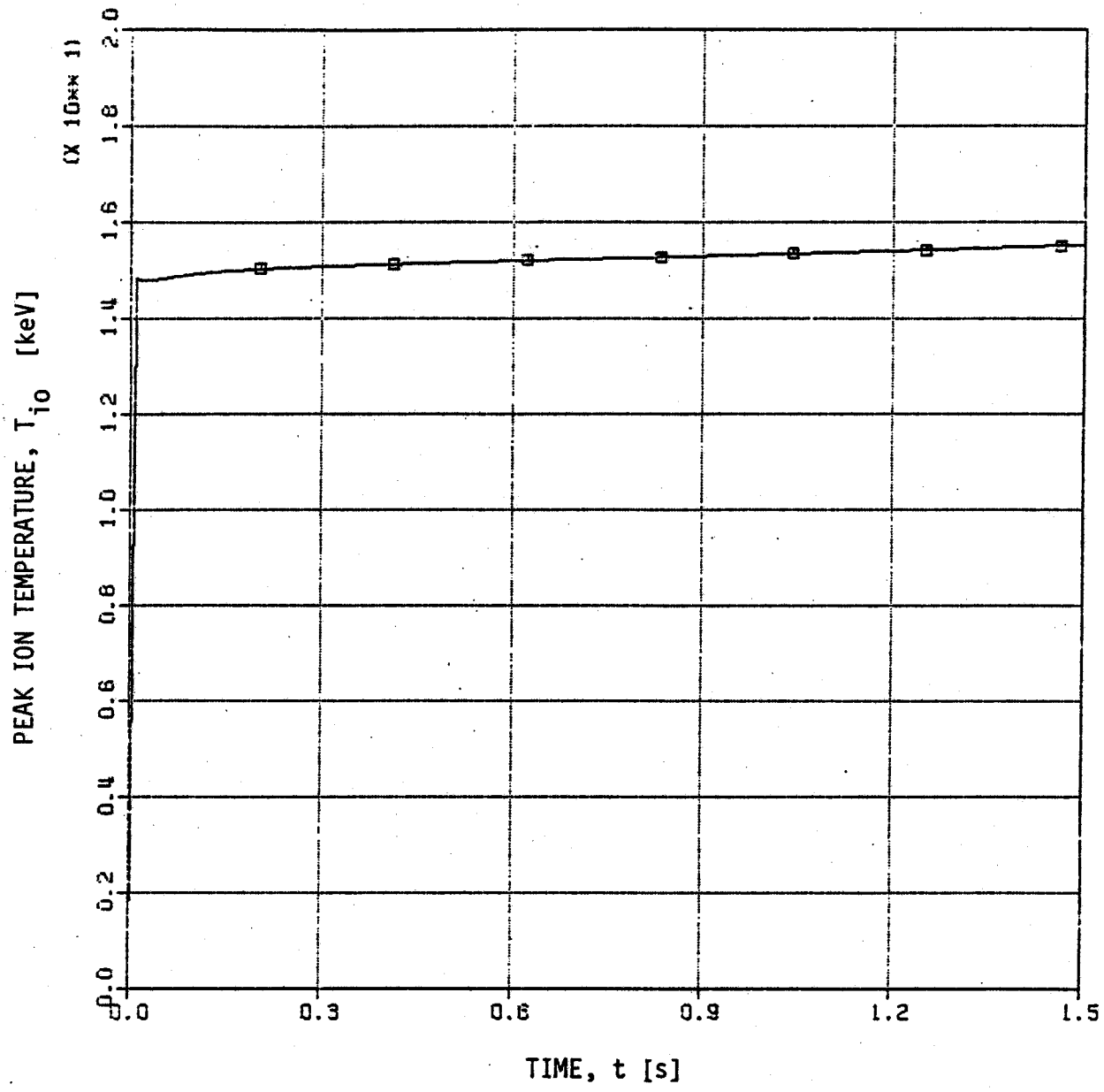
PEAK ION TEMPERATURE, T_{io} [keV]
(X 10** 1)
2.0
1.8
1.6
1.4
1.2
1.0
0.8
0.6
0.4
0.2
0.0
0.0
0.3
0.6
0.9
1.2
1.5
TIME, t [s]

Fig. 12b

PFC BASE LIST

INTERNAL MAILINGS (MIT)

G. Bekefi
36-213

A. Bers
38-260

D. Cohn
NW16-250

B. Coppi
26-201

R.C. Davidson
NW16-202

T. Dupree
38-172

S. Foner
NW14-3117

J. Freidberg
38-160

A. Gondhalekar
NW16-278

M.O. Hoenig
NW16-176

M. Kazimi
NW12-209

L. Lidsky
38-174

E. Marmar
NW16-280

J. McCune
31-265

J. Meyer
24-208

D.B. Montgomery
NW16-140

J. Moses
NE43-514

D. Pappas
NW16-272

R.R. Parker
NW16-288

N.T. Pierce
NW16-186

P. Politzer
NW16-286

M. Porkolab
36-293

R. Post
NW21-

H. Praddaude
NW14-3101

D. Rose
24-210

J.C. Rose
NW16-189

R.M. Rose
4-132

B.B. Schwartz
NW14-5121

R.F. Post
NW21-203

L.D. Smullin
38-294

R. Temkin
NW16-254

N. Todreas
NW13-202

J.E.C. Williams
NW14-3210

P. Wolff
36-419

T.-F. Yang
NW16-164

Industrial Liaison Office
ATTN: Susan Shansky
Monthly List of Publications
39-513

MIT Libraries
Collection Development
ATTN: MIT Reports
14E-210

B. Colby
PFC Library
NW16-255

EXTERNAL MAILINGS

National

Argonne National Laboratory
Argonne, IL 60439
ATTN: Library Services Dept.

Battelle-Pacific Northwest Laboratory
P.O. Box 99
Richland, WA 99352
ATTN: Technical Information Center

Brookhaven National Laboratory
Upton, NY 11973
ATTN: Research Library

U.S. Dept. of Energy
Washington, D.C. 20545
ATTN: D.O.E. Library

Roger Derby
Oak Ridge National Lab.
ETF Design Center
Bldg. 9204-1
Oak Ridge, TN 37830

General Atomic Co.
P.O. Box 81608
San Diego, CA 92138
ATTN: Library

Lawrence Berkeley Laboratory
1 Cyclotron Rd.
Berkeley, CA 94720
ATTN: Library

Lawrence Livermore Laboratory
UCLA
P.O. Box 808
Livermore, CA 94550

Oak Ridge National Laboratory
Fusion Energy Div. Library
Bldg. 9201-2, ms/5
P.O. Box "Y"
Oak Ridge, TN 37830

Dr. D. Overskei
General Atomic Co.
P.O. Box 81608
San Diego, CA 92138

Princeton Plasma Physics Laboratory
Princeton University
P.O. Box 451
Princeton, NJ 08540
ATTN: Library

Plasma Dynamics Laboratory
Jonsson Engineering Center
Rensselaer Polytechnic Institute
Troy, NY 12181
ATTN: Ms. R. Reep

University of Wisconsin
Nuclear Engineering Dept.
1500 Johnson Drive
Madison, WI 53706
ATTN: UV Fusion Library

EXTERNAL MAILINGS

International

Professor M.H. Brennan
Willis Plasma Physics Dept.
School of Physics
University of Sydney
N.S.W. 2006, Australia

Division of Plasma Physics
Institute of Theoretical Physics
University of Innsbruck
A-6020 Innsbruck
Austria

c/o Physics Section
International Atomic Energy Agency
Wagramerstrasse 5
P.O. Box 100
A-1400 Vienna, Austria

Laboratoire de Physique des Plasmas
c/o H.W.H. Van Andel
Dept. de Physique
Universite de Montreal
C.P. 6128
Montreal, Que H3C 3J7
Canada

Plasma Physics Laboratory
Dept. of Physics
University of Saskatchewan
Saskatoon, Sask., Canada S7N OWO

The Library
Institute of Physics
Chinese Academy of Sciences
Beijing, China

Mrs. A. Wolff-Degives
Kernforschungsanlage Julich GmbH
Zentralbibliothek - Exchange Section
D-5170 Julich - Postfach 1913
Federal Republic of Germany

Preprint Library
Central Research Institute for Physics
H-1525 Budapest, P.O. Box 49
Hungary

Plasma Physics Dept.
Israel Atomic Energy Commission
Soreq Nuclear Research Center
Yavne 70600
Israel

The Librarian (Miss DePalo)
Associazione EURATOM - CNEN Fusione
C.P. 65-00044 Frascati (Rome)
Italy

Librarian
Research Information Center
Institute of Plasma Physics
Nagoya University
Nagoya, 464
Japan

Dr. A.J. Hazen
South African Atomic Energy Board
Private Bag X256
Pretoria 0001
South Africa